GEORGIA INSTITUTE OF TECHNOLOGY
OFFICE OF CONTRACT ADMINISTRATION
SPONSORED PROJECT INITIATION

Date: __August 18, 1978__

Project Title: A Numerical Model of the Interaction of Density Currents and Wind-Induced Mixing in Stratified Cooling Lakes

Project No: E-20-643

Project Director: Dr. T. W. Sturm

Sponsor: National Science Foundation

Agreement Period: From ___9/1/78___ Until ___8/31/80___
(Includes 6-months unfunded flexibility period)

Type Agreement: Grant No. ENG78-21957

Amount:
$23,000 (NSF - E-20-643)
_9,847_ (GIT - E-20-314)
$32,487 TOTAL

Reports Required: Final Project Report

Sponsor Contact Person (s):

Technical Matters	Contractual Matters (thru OCA)
Arthur A. Ezra Water Resources, Urban and Environmental Engineering Program National Science Foundation Washington, D. C. (202) 632-5787	Mary Frances O'Connell, Grants Officer MPE/BBS/SE Branch National Science Foundation Washington, D. C. (202) 632-2858

Defense Priority Rating: N/A

Assigned to: ___Civil Engineering___ (School/Laboratory)

COPIES TO:

Project Director
Division Chief (EES)
School/Laboratory Director
Dean/Director—EES
Accounting Office
Procurement Office
Security Coordinator (OCA)
Reports Coordinator (OCA)

Library, Technical Reports Section
EES Information Office
EES Reports & Procedures
Project File (OCA)
Project Code (GTRI)
Other_____

CA-3 (3/76)

GEORGIA INSTITUTE OF TECHNOLOGY

OFFICE OF CONTRACT ADMINISTRATION

SPONSORED PROJECT TERMINATION

Date: April 13, 1981

Project Title: A Numerical Model of the Interaction of Density Currents
and Wind-Induced Mixing in Stratified Cooling Lakes

Project No: E-20-643

Project Director: Dr. T. W. Sturm

Sponsor: National Science Foundation, Washington, DC

Effective Termination Date: ____8/31/80____

Clearance of Accounting Charges: ___8/31/80___

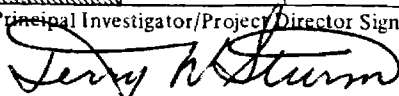Grant/Contract Closeout Actions Remaining:

- x_ Final Invoice ~~and Closing Documents~~
- x_ Final Fiscal ~~Report~~ Accounting (FCTR)
- _ Final Report of Inventions
- _ Govt. Property Inventory & Related Certificate
- _ Classified Material Certificate
- _ Other _____

Assigned to: __Civil Engineering_____ (School/~~Laboratory~~)

COPIES TO:

Project Director
Division Chief (EES)
School/Laboratory Director
Dean/Director—EES
Accounting Office
Procurement Office
Security Coordinator (OCA)
Reports Coordinator (OCA)

Library, Technical Reports Section
EES Information Office
Project File (OCA)
Project Code (GTRI)
Other_____

CA—4 (1/79)

E-20-643

PLEASE READ INSTRUCTIONS ON REVERSE BEFORE COMPLETING

PART I—PROJECT IDENTIFICATION INFORMATION

1. Institution and Address	2. NSF Program Water Resources	3. NSF Award Number
School of Civil Engineering Georgia Institute of Technology Atlanta, Georgia 30332	Urban and Env. Engr.	ENG 78-21957
	4. Award Period From 9/1/78 To 8/31/80	5. Cumulative Award Amount $23,000

6. Project Title

A Numerical Model of the Interaction of Density Currents
and Wind-Induced Mixing in Stratified Cooling Lakes

PART II—SUMMARY OF COMPLETED PROJECT (FOR PUBLIC USE)

The effects of wind and density (gravity) currents on the thermal structure and surface heat loss characteristics of cooling lakes are considered in this research. A closed-form solution for laminar density currents in cooling lake sidearms is presented and verified with laboratory data. A surface wind stress directed toward the dead end of the sidearm is added to the density current problem formulation and the governing momentum and thermal energy conservation equations are solved numerically. The numerical results are used to develop a surface heat loss relation for a combined wind-driven and density current circulation in a cooling lake sidearm. The surface stirring effect of wind on developing stratification in a cooling lake is also considered. A computer simulation model is developed to include the effects of wind mixing, vertical advection due to cooling water circulation, and surface heat loss on determining daily vertical temperature profiles in a cooling lake. The model is applied to a field cooling lake after being calibrated on an adjacent natural lake. The simulation model results are compared to field temperature data, and the dominance of vertical advection over wind mixing is clearly shown. Dimensionless parameters for assessing the relative influence of wind mixing and vertical advection are suggested. These research results provide an aid to future comprehensive modeling efforts which include the various effects of wind and density currents on the thermal structure of cooling lakes.

PART III—TECHNICAL INFORMATION (FOR PROGRAM MANAGEMENT USES)

1. ITEM (Check appropriate blocks)	NONE	ATTACHED	PREVIOUSLY FURNISHED	TO BE FURNISHED SEPARATELY TO PROGRAM Check (✓)	Approx. Date
a. Abstracts of Theses	X				
b. Publication Citations		X			
c. Data on Scientific Collaborators		X			
d. Information on Inventions	X				
e. Technical Description of Project and Results		X			
f. Other (specify)					

2. Principal Investigator/Project Director Name (Typed)	3. Principal Investigator/Project Director Signature	4. Date
Terry W. Sturm	*Terry W. Sturm*	3/20/81

b. <u>Publication Citations</u>

"Laminar Gravitational Convection of Heat in Dead-End
      Channels," accepted for publication in Journal of
      Fluid Mechanics, in press.

"Thermal Water Quality in Stratified Cooling Lakes,"
      accepted for publication in Proceedings, National
      ASCE Environmental Engineering Conference, Atlanta,
      Georgia, July, 1981.

"Combined Wind-Driven and Gravitational Circulations
      in Dead-End Channels," to be submitted for publi-
      cation in ASCE Journal of Engineering Mechanics,
      April, 1981.

c. <u>Data on Scientific Collaborators</u>

Richard Luettich, graduate student research assistant.

Janice Fulford, graduate student research assistant

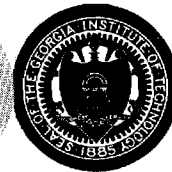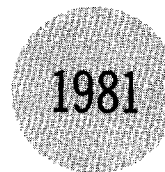FINAL REPORT
PROJECT NO. E–20–643
NSF GRANT NO. ENG78–21957

A NUMERICAL MODEL OF THE INTERACTION OF DENSITY CURRENTS AND WIND–INDUCED MIXING IN STRATIFIED COOLING LAKES

By

Terry W. Sturm

Prepared for

NATIONAL SCIENCE FOUNDATION

MARCH 1981

GEORGIA INSTITUTE OF TECHNOLOGY
SCHOOL OF CIVIL ENGINEERING
ATLANTA, GEORGIA 30332

1981

A NUMERICAL MODEL OF THE
INTERACTION OF DENSITY CURRENTS
AND WIND-INDUCED MIXING IN
STRATIFIED COOLING LAKES

Final Report

by

Terry W. Sturm

prepared for

School of Civil Engineering
Georgia Institute of Technology
Atlanta, Georgia 30332

March 1981

ABSTRACT

The effects of wind and density (gravity) currents on the thermal
structure and surface heat loss characteristics of cooling lakes are
considered in this report. A closed-form solution for laminar density
currents in cooling lake sidearms is presented and verified with lab-
oratory data. A surface wind stress directed toward the dead end
of the sidearm is added to the density current problem formulation
and the governing momentum and thermal energy conservation equations
are solved numerically. The numerical results are used to develop a
surface heat loss relation for a combined wind-driven and density
current circulation in a cooling lake sidearm. The surface stirring
effect of wind on developing stratification in a cooling lake is
also considered. A computer simulation model is developed to include
the effects of wind mixing, vertical advection due to cooling water
circulation, and surface heat loss on determining daily vertical
temperature profiles in the cooling lake. The model is applied to a
field cooling lake after being calibrated on an adjacent natural lake.
The simulation model results are compared to field temperature data,
and the dominance of vertical advection over wind mixing is clearly
shown. Dimensionless parameters for assessing the relative influence
of wind mixing and vertical advection are suggested. These research
results provide an aid to future comprehensive modeling efforts which
include the various effects of wind and density currents on the thermal
structure of cooling lakes.

ACKNOWLEDGEMENTS

TABLE OF CONTENTS

LIST OF FIGURES

LIST OF TABLES

LIST OF SYMBOLS

A_s Lake surface area

B Average lake width at level of outlet

b Sidearm width

C_D Water surface drag coefficient for wind

$D(x)$ Sidearm depth at any x

D_i Sidearm depth at $x = 0$

F_D Outflow or withdrawal densimetric Froude number

$f_u(\eta)$ Velocity profile polynomial for wind-driven currents

$f_T(\eta)$ Assumed temperature profile

$f_w(\eta)$ Velocity profile polynomial for wind-driven currents

H_E Total rate of surface heat loss for $L = L_e$

H_L Total rate of surface heat loss for sidearm of length L

H' H_L/H_E

K Local coefficient of surface heat transfer

L Sidearm length

L_e Equilibrium length required for $T_o = T_e$

q_i Discharge per unit width into sidearm at $x = 0$

Ra_m Modified Rayleigh number

Ri_* Wind Richardson number

r_c Critical ratio of wind kinetic energy and buoyant potential energy for entrainment

S_w $\tau_s/\gamma_w D$

T_i Surface temperature at $x = 0$

T_o Surface temperature at $x = L$

T_e	Equilibrium temperature
$T_s(x)$	Surface temperature at any x
u_s	Surface velocity
u_{si}	Surface velocity at $x = 0$
u_*	$(\tau_s/\rho_w)^{1/2}$
U_s	u_s/u_{si}
V_w	Wind speed
γ	L/L_e
γ_w	Specific weight of water
δ	D/D_i
η	y/D
ψ	Coefficient in evaporative heat flux formula
ψ_{PL}	Pretty Lake formula
ψ_Z	Zaykov formula
ρ_o	Density at $T = T_o$
ρ_e	Density at $T = T_e$
$\Delta\rho_o$	$\rho(T_o) - \rho(T_i)$
$\Delta\rho_e$	$\rho(T_e) - \rho(T_i)$
ρ_w	Density of water
ρ_a	Density of air
ϕ_n	Net surface heat loss rate
ϕ_e	Evaporative heat flux
σ_o	Outflow distribution standard deviation
σ_I	Inflow distribution standard deviation

θ_e $\qquad (T_s - T_e)/(T_i - T_e)$

θ_o $\qquad (T_o - T_e)/(T_i - T_e)$

θ_s $\qquad (T_s - T_o)/(T_i - T_o)$

τ_s $\qquad$ Surface wind shear stress

1. INTRODUCTION

National concern for conservation of existing water resources suggests the possibility of utilizing multiple-purpose reservoirs and lakes as cooling water sources for the dissipation of waste heat from steam generation of electric power. Existing lakes and reservoirs could conceivably be used conjunctively with wet cooling towers to obtain an optimum cooling system which makes the most efficient use of existing water resources subject to environmental constraints. Scherer (1975) has suggested that the least-cost cooling system may consist of utilizing a lake for "once-through" cooling up to a critical condensor flow rate, at which the marginal costs of lake and cooling-tower systems are equal, and then passing the condensor flow rate in excess of the critical value through cooling towers. Giquinta et al. (1980) studied the economics of several hybrid cooling systems at river sites and concluded that the hybrid systems, which included both once-through river cooling and cooling towers, were economically superior to once-through cooling alone.

· If cooling towers are used conjunctively with cooling lakes for the dissipation of power plant waste heat, the impact of such a system on the environment must be considered. Not only must thermal water quality standards be met at the cooling water discharge point in the lake, but the effect of the cooling system on the long-term thermal structure of the lake, and hence the effect of this water use on other beneficial uses and on the lake biota, must be evaluated. If, for example, the thermocline is deepened by cooling water circulations in the lake, the thermal niche of certain types of fish may be adversely affected. This becomes an environmental constraint which must be satisfied in the optimization of the hybrid cooling system.

Evaluation of thermal environmental constraints for a cooling lake requires a thorough knowledge of the physical mechanisms responsible for the thermal structure of a cooling lake. In a natural lake, the establishment of the depth of the thermocline depends upon an energy balance between the kinetic energy supplied by wind and the buoyant potential energy of density stratification. Coooling water discharges and withdrawals from a lake by a power plant tend to have an additional important influence on the location of the thermocline and hence on the size and temperature of the epilimnion. This influence is manifested by two separate physical mechanisms: (1) the vertical advection of heat caused by heated discharges near the lake surface and withdrawal from lower, cooler layers; and (2) the dispersion of heat at the lake surface by wind-induced currents, through-flow currents, and density currents. The manner in which heat is dispersed at the lake surface is linked to the amount of surface heat loss and thus also to the balance between wind kinetic energy and buoyant potential energy.

The research reported herein specifically considers the interaction of wind-driven and density currents as well as the direct influence of wind in establishing the vertical thermal structure of a cooling lake. Density currents develop in sidearms of cooling lakes as a result of the horizontal temperature gradients, and hence density gradients, that are sustained in the sidearm by surface cooling. The resulting gravitational circulation acts as a heat pump which delivers heat from the main body of the cooling lake into sidearms where it is lost to the atmosphere. The heat pump is self-sustaining because surface cooling maintains the horizontal temperature gradient

necessary for its existence. If a surface wind stress is superimposed

on this density current, the amount of heat carried into the sidearm

by longitudinal advection is affected. At the same time, the wind

also influences the rate of heat loss from the water surface and

thus affects the magnitude of the driving buoyant force. A third

influence of the wind is manifested by the kinetic energy generated

by surface stirring that becomes available for deepening of the

thermocline. In this manner the wind affects the vertical temperature

profile in the main body of the lake and at the entrance to the sidearm.

These three influences of wind on the thermal structure of a cooling

lake are studied in detail in this report.

First, the density-current (gravity current) problem is formulated

for the case of laminar flow and no surface wind stress. A closed-

form solution is obtained for this case, and the results are compared

to experimental results from previous research. Second, the problem

is reformulated with an imposed surface wind stress directed toward the

dead end of the sidearm. In this case, the governing equations are

solved numerically, and the results are compared to the closed-form

solution. In addition, the results are applied to develop the concept

of a limiting wind speed beyond which the wind-driven currents over-

power the gravity currents. Third, a daily computer simulation model is

developed to model the influence of wind on the daily mean vertical

temperature profile in a cooling lake which receives power-plant condensor

discharges both directly from the condensors and indirectly through a

cooling tower system. Finally, the simulation model is applied for a set of

field temperature data measured in two adjacent lakes, one of which

is used as a cooling lake, on the University of Notre Dame campus.

2. LAMINAR GRAVITY CURRENTS

2.1 Introduction

In this chapter and in following chapters, the term gravity current is used synonymously with the term density current. The latter term is used often in the Civil Engineering literature, but the former is preferred because it is more descriptive of the causative force driving such flows. The distinguishing characteristic of gravity currents is that they are driven by a buoyancy which is the result of a density gradient in a gravitational field. The gravity currents of interest in this report are associated with thermally-induced density gradients that occur in cooling lakes. These gravity currents are of particular interest in dead-end channels, or sidearms, that form a portion of a natural lake used for cooling water. The gravitational circulation tends to draw heated water into "stagnant" areas of the lake where it undergoes surface cooling that sustains the circulation. The gravity current problem is formulated in this chapter without consideration of wind stress, and a closed-form solution is obtained that was found useful in interpreting the results in the following chapter where wind stress is considered.

Benjamin (1968) has clearly demonstrated the role of gravity in generating a streamwise pressure gradient where there exists a difference in fluid density in the direction of flow. This manifestation of the gravity force is distinct from its role as a body force. Even though the channel slope is zero with a resulting zero component of the body force in the direction of flow, buoyancy can drive a circulation as in the familiar example of lock-exchange flow between fresh-water and saline-water canals (Keulegan, 1957).

The work by Phillips (1966) on the gravitational circulation of the Red Sea showed that a similarity solution of the turbulent equations of motion is possible when the surface buoyancy flux due to salt and heat flux is considered to be independent of the streamwise coordinate. Imberger (1974) studied laminar gravitational circulation experimentally, but in his case the end walls of the channel were differentially heated and the flow was confined at the top by an insulated lid. In a companion theoretical investigation of this problem, Cormack, Leal, and Imberger (1974) applied an asymptotic analysis to the case of fixed Rayleigh number with the aspect ratio of the enclosed cavity approaching zero. Their analysis indicated the existence of a parallel flow structure in the core of the cavity.

The essential aspect of the gravity currents considered herein is the continuous change in the thermally-induced density gradient in the direction of flow as controlled by the heat transfer process at the free surface. This type of gravitational circulation depends upon the coupling between the equations of motion and the equation of thermal energy conservation. The surface heat flux is not only a component in the thermal energy balance but determines the horizontal pressure gradient in the equations of motion as well.

Gravity currents which are the result of thermally-induced density gradients that are diminished by surface heat flux have been studied experimentally by Brocard, Jirka, and Harleman (1977) and by the author (Sturm, 1976). The analytical work by the author (Sturm, 1976) led to a numerical solution of the governing equations of motion and thermal energy for both laminar and turbulent circulations. The occurrence of the laminar regime in the laboratory provided the impetus to seek a closed-form solution for the laminar case which could be compared with solutions including surface wind stress as given in the following chapter.

2.2 Formulation

The problem is formulated with reference to the dead-end channel sketched in Figure 1. The channel is assumed to have a horizontal bottom, a uniform width b, length L, and depth $D(x)$, where the coordinate system is defined in the figure. At the entrance to the channel ($x = 0$), there is a vertically nonuniform temperature profile with a surface temperature $T_s = T_i$ and a bottom temperature $= T_o$. Based on the experiments of the author (Sturm, 1976), which will be discussed subsequently, it can be assumed that the temperature reached by the surface inflow current at the dead end of the channel becomes equal to the constant temperature T_o of the bottom outflow current.

The surface heat-loss rate, ϕ_n, depends on the water surface temperature, T_s, and decreases with x as surface cooling occurs in the inflow current shown in Figure 1. If essentially parallel flow is considered to exist in a central region of the channel, then a comparison of the hydrostatic pressure distributions at each end of this central region reveals a net force directed toward the open end of the channel. This force propels the bottom outflow current in Figure 1. Continuity requires an equal but opposite inflow current which rides over the top of the outflow current. The inflow current must be driven by a drop in the free surface toward the dead end of the channel. The central region of the channel is bounded by a flow-establishment region near the channel entrance in which inertia and buoyancy forces are dominant, and a dead-end region which is characterized by a large vertical downflow as the inflow current is turned. The analysis herein is concerned primarily with the central region of a dead-end channel with large length-to-depth ratio in which the flow is nearly parallel and governed by buoyancy and viscous forces.
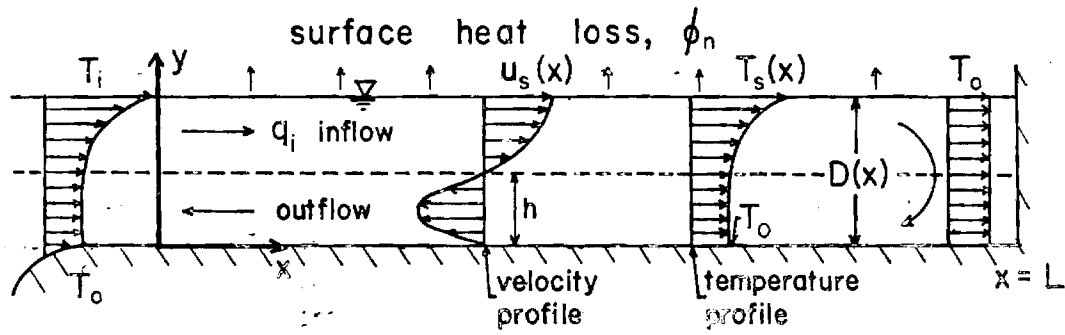
Fig. I - Section of Gravity Current in Dead-End Channel.

The equations of motion and thermal energy conservation are simplified by making the following assumptions: (1) the flow is laminar; (2) the dead-end channel has a large length-to-depth ratio (small aspect ratio); (3) the rate of surface heat loss, ϕ_n, can be related linearly to the excess surface temperature relative to an equilibrium temperature, T_e, e.g., $\phi_n = -K(T_s-T_e)$; (4) the vertical temperature profile shape is known and can be expressed by $\theta = (T-T_o)/(T_s-T_o) = f_T(\eta)$ where $\eta = y/D$; (5) the temperature vs. density relation is approximately linear over the surface temperature range, (T_i-T_o); and (6) the Boussinesq assumption applies.

Although the assumption of laminar flow may be unrealistic except in laboratory situations, it is made in order to gain some insight into the more complex dynamics of turbulent gravity currents, which occur in cooling lakes. In the central region of the flow, which is relatively very long in comparison to the depth as supposed by assumption (2), boundary-layer-type simplifications become possible in the equations of motion and thermal energy. The linear relation for ϕ_n in assumption (3) is based on an equilibrium temperature, T_e, such that when $T_s = T_e$, there is no net surface heat flux. The coefficient, K, and T_e are functions of meteorological conditions and the surface temperature at x=0, T_i. They can be determined by the empirical relations summarized by Ryan et al. (1974) for the relevant processes of heat transfer at the air-water interface. Assumption (4) concerning the temperature profile shape is similar to that employed in the Kármán-Pohlhausen type of boundary layer analysis in which the integral properties of the flow in the vertical direction are retained to effect a solution with respect to the horizontal, streamwise coordinate.

With the above assumptions, the coupled equations of motion and thermal energy become:

$$\rho_o(u\,\frac{\partial u}{\partial x} + v\,\frac{\partial u}{\partial y}) = -\,\frac{\partial p}{\partial x} + \mu\frac{\partial^2 u}{\partial y^2} \tag{1}$$

$$\frac{\partial p}{\partial y} = -\rho g = -g(\alpha T + \beta) \tag{2}$$

$$\frac{d}{dx}\int_0^D uT\,dy = \frac{-K}{\rho_o c_p}(T_s - T_e) \tag{3}$$

in which ρ_o is a reference density corresponding to the temperature, T_o, and α is the slope of the density vs. temperature relation. The thermal energy equation, (3), has been written in integral form by applying the continuity equation and integrating over the depth with a boundary condition of zero heat flux at $y = 0$, and with the heat flux being given by the assumed linear relation at the air-water interface $(y = D)$.

The inertia terms have been retained in (1) based on a preliminary order-of-magnitude analysis, while the horizontal diffusive terms have been neglected in (1) and (3) in comparison with the corresponding vertical contributions because $L/D >> 1$. A closer examination of the horizontally-elongated central region of the dead-end channel, however, reveals that the inertia terms may make a sufficiently small contribution to equation (1) to be neglected as a first approximation. If the channel is very long (i.e., sufficiently long that all excess heat is lost to the atmosphere), the long-itudinal gradient of horizontal velocity is quite small as is the magnitude of the velocity itself. For a shorter channel which still has a large length-to-depth ratio, much of the inertia of the inflow current might be expected to be lost within a horizontal distance of a few depths from the dead end of the channel. In this end region, which is very short, the inertia of the inflow current is lost rapidly as the dead end is approached and the free surface rises. The inertia is regained as the outflow current accelerates from the dead end and flows in a direction opposite to that of

the inflow current. Thus, in the central region of essentially parallel flow, the inertia terms may be sufficiently small, when compared to the buoyancy and viscous forces, to be neglected. This assumption cannot be verified *a priori* because a careful estimate of the velocity scale can only be made after a solution of this free convection problem has been obtained.

Buoyant flows for which the formulation is given by (1)-(3), excluding the inertia terms in (1), have been classified by Turner (1973) as viscous diffusive flows. Turner points out that this type of flow can be characterized by a single dimensionless parameter, the Rayleigh number, which reflects the importance of diffusion as well as viscous and buoyancy forces. Such a formulation corresponds to Koh's (1966) zeroth order approximation for the problem of viscous stratified flow towards a sink. As another example of this type of flow, data for free-convection heat transfer from horizontal cylinders in several different fluids are well correlated with the Rayleigh number as the only independent parameter (Kreith, 1973).

As a first approximation, then, it is not without precedent nor lacking in at least some intuitive justification to neglect the inertia terms in (1) for the problem under consideration. This is done in the following section of this paper in which a closed-form solution of (1)-(3) is presented. The limitations of this assumption will be analyzed in more detail in §2.4.

2.3 Solution

The solution of (1), (2), and (3), with the inertia terms neglected in (1), proceeds by substituting the temperature profile function $f_T(\eta)$ into (2) and eliminating the pressure p from (1) and (2) to obtain:

$$\frac{\partial^2 u}{\partial y^2} = -\frac{\alpha g D}{\mu} \frac{d(T_s - T_o)}{dx} \int_1^\eta f_T(\eta)d\eta + \frac{g(\alpha T_o + \beta)}{\mu} \frac{dD}{dx} \qquad (4)$$

Equation 4 is integrated with the boundary conditions u=0 at y=0 and $\partial u/\partial y = 0$ at y=D to produce the velocity distribution:

$$u = \frac{\alpha g D^3}{\mu} \frac{d(T_s - T_o)}{dx} f_u(\eta) \qquad (5)$$

where dD/dx has been expressed in terms of the temperature gradient, $d(T_s - T_o)$ /dx, by applying the continuity condition, $\int_0^1 u \, d\eta = 0$.

The function $f_u(\eta)$ in (5) is a velocity profile function determined solely by the choice of the temperature profile shape, $f_T(\eta)$. In Figure 2, $f_u(\eta)$ is shown for $f_T(\eta) = \eta^2$ and $f_T(\eta) = \eta^4$. The postulated counter-flow is readily evident from the shape of $f_u(\eta)$. The elevation of zero velocity between the inflow and outflow currents is relatively insensitive to the choice of $f_T(\eta)$, but the magnitude of $f_u(\eta)$ decreases at all elevations with an increase in the degree of the temperature profile polynomial, $f_T(\eta)$.

The solution given by (5) for the velocity u was obtained solely from momentum and continuity considerations, and it involves the surface temperature gradient, $d(T_s - T_o)/dx$, as an unknown parameter. This parameter couples the momentum equation to the thermal energy equation. If (5) is substituted into (3), which is the thermal energy equation, along with the
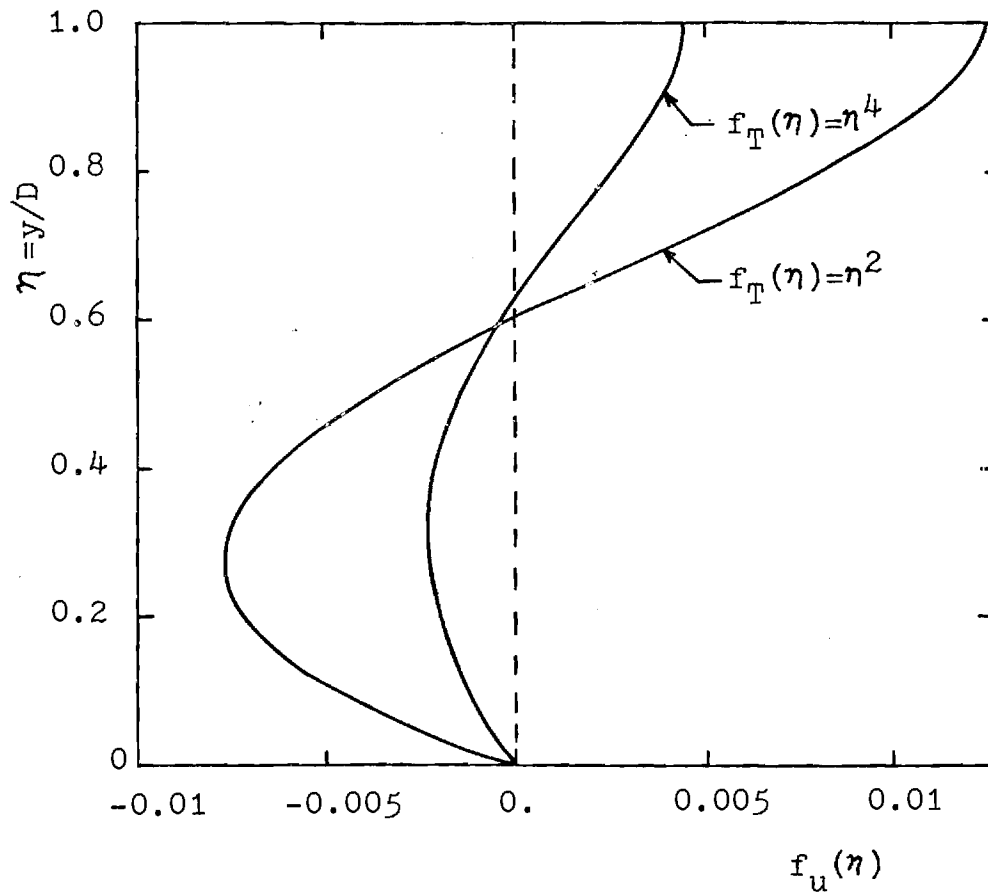
Figure 2. – Velocity Profile Polynomials for
Different Temperature Profile Assumptions

assumed temperature profile $f_T(\eta)$, then there results an ordinary differential equation in the unknown $(T_s - T_o)$. In dimensionless form, the equation to be solved is:

$$\theta_s \frac{d^2\theta_s}{dx^{\circ 2}} + \left(\frac{d\theta_s}{dx^\circ}\right)^2 - B_1\theta_s - \frac{B_1\theta_o}{(1-\theta_o)} = 0 \tag{6}$$

where

$$x^\circ = \frac{x}{D}; \quad \theta_s = \frac{(T_s - T_o)}{(T_i - T_o)}; \quad \theta_o = \frac{(T_o - T_e)}{(T_i - T_e)};$$

$$B_1 = \frac{C_1}{Ra_m(1-\theta_o)}; \quad Ra_m = \frac{(\Delta\rho_e/\rho_e)gD_i^2}{\nu K/\rho_e c_p}$$

and where an i subscript refers to values at x=0; ν is kinematic viscosity; K is the local surface heat transfer coefficient; c_p is specific heat; g is gravitational acceleration; C_1 is a temperature profile constant defined in the appendix; $\Delta\rho_e = \rho(T_e) - \rho(T_i)$; $\rho_e = \rho(T_e)$; and the various temperatures are defined in Figure 1.

The governing dimensionless parameter in (6) is a modified form of the Rayleigh number, Ra_m, in which the thermal conductivity has been replaced by KD_i. The local coefficient of heat transfer $K[= -\phi_n/(T_s-T_e)]$ characterizes all the heat transfer processes at the air-water interface including evaporation, conduction, and radiation. The modified Rayleigh number can be considered to be a product of the Grashof number and a modified Prandtl number given by $\mu c_p/KD_i$. The additional parameter

appearing in (6) is θ_o, which is the unknown temperature boundary condition

at x=L, where L is the channel length. It will be shown below that θ_o can

be determined as a function of L, D_i, and Ra_m.

An exact solution can be obtained for (6) by making the substitution

of variables $\chi = d\theta_s/dx^o$ with θ_s becoming the independent variable and χ

the dependent variable. Exact integration of (6) with the boundary con-

ditions $\theta_s = 1$ at $x^o = 0$ and $d\theta_s/dx^o$ finite as θ_s approaches zero provides

the solution for the dimensionless temperature, velocity, and depth:

$$\theta_s = \frac{T_s - T_o}{T_i - T_o} = \frac{B_1}{6} x^{o\,2} - B_2 x^o + 1 \tag{7}$$

$$U_s = \frac{u_s}{u_{si}} = 1 - \frac{B_1}{3B_2} x^o \tag{8}$$

$$\delta = \frac{D(x)}{D_i} = 1 - C_2 \frac{\Delta\rho_o}{\rho_o} x^o \left[B_2 - \frac{B_1}{6} x^o \right] \tag{9}$$

where

$$B_2 = \left(\frac{B_1^2 L^{o\,2}}{36} + \frac{B_1}{3} + \frac{1}{L^{o\,2}} \right)^{\frac{1}{2}} ;$$

and where $L^o = L/D_i$; C_2 is a temperature profile constant defined in the

appendix; $\Delta\rho_o = \rho(T_o) - \rho(T_i)$; and the other variables are as defined

previously. The solution given by (8) for U_s is determined by differen-

tiating (7) with respect to x^o and substituting the result into (5). The

continuity condition and the integrated form of (4) provide the necessary

relation between $d\theta_s/dx°$ and $d\delta/dx°$ from which (9) is obtained.

The solutions given by (7), (8), and (9) are not complete without the boundary values of the surface velocity at x=0, u_{si}, and the surface temperature at x=L, T_o. These must be determined from the imposed physical conditions of channel length, depth, surface temperature at the channel entrance, and meteorology.

The unknown boundary condition θ_o for a channel of given length L is determined by setting $T_s = T_o$ at x=L in (7) and expressing the result in terms of the ratio $\gamma = L/L_e$, where L_e is an equilibrium length:

$$\theta_o = 1 + 2\gamma^2 - \gamma(6 + 3\gamma^2)^{\frac{1}{2}} \tag{10}$$

The equilibrium length is defined to be the length of channel required for the surface temperature T_s to become equal to T_e, the equilibrium temperature, at which the net surface heat exchange is zero. The equilibrium length is determined from (7) as the value of x for which $T_s = T_o = T_e$:

$$\frac{L_e}{D_i} = \left(\frac{6\ Ra_m}{C_1}\right)^{\frac{1}{2}} \tag{11}$$

It is now apparent from (10) and (11) that the dimensionless boundary value given by θ_o is a function only of L/D_i, the Rayleigh number, and the profile constant C_1.

The inlet surface velocity, u_{si}, is easily determined from (5) and (7):

$$\frac{u_{si}}{K/\rho_e c_p} = C_3 \frac{B_2}{B_1} \tag{12}$$

where C_3 is another temperature profile constant defined in the appendix, and B_2 and B_1 are as defined before. For the purpose of later comparison with experimental data, it is more convenient to use an expression for the inflow per unit width into the channel, q_i:

$$q_i' = \frac{q_i}{\left(\frac{KL_e}{\rho_e c_p}\right)} = C_4 \frac{B_2}{B_1 L_e^\circ} \tag{13}$$

where C_4 is defined in the appendix and $L_e^\circ = L_e/D_i$. It can also be shown that $B_2/B_1 L_e^\circ$ and hence q_i' are functions only of $\gamma = L/L_e$ just as for θ_o.

Although the solution of (1), (2), and (3) is now complete, one of the quantities of interest may be the total rate of surface heat loss from the channel, which can be determined from the foregoing development. If the total rate of surface heat loss H_E from a channel of equilibrium length and width b is defined as

$$H_E = b \int_0^{L_e} \phi_n \, dx = \bar{h}_c \, b \, L_e \, (T_i - T_e), \tag{14}$$

it is readily shown that $\bar{h}_c = K/3$ from a substitution of (7) into (14). For a channel of specified length L, the ratio of surface heat-loss rate H_L to that from the equilibrium channel of length L_e is formed and found to be a function of $\gamma = L/L_e$:

$$H' = \frac{H_L}{H_E} = 3\gamma \left[1 + \frac{\gamma^2}{3} - \left(\gamma^4 + \frac{3\gamma^2}{2} - \frac{\gamma^3}{2} (6 + 3\gamma^2)^{1/2} \right)^{1/2} \right] \tag{15}$$

The solutions for θ_o, q_i', and H' are shown in Figure 3 as a function of γ.

The profile constants that appear in the solution are given in Table 1 for several polynomial temperature profile shapes. The shapes chosen are $f_T (\eta)$ = η^m where m varies from one to five. These functions were selected for ease of integration. Other functions are possible, and the resulting constants can be evaluated from the expressions given in the appendix. Because of the way in which the surface heat transfer boundary condition is specified in the integral solution approach, it is unnecessary for the assumed temperature profile shape to have the correct slope at the free surface.

2.4 Discussion of Solution

Introduction of the equilibrium length L_e provides a useful generalization of the dimensionless solutions for surface temperature, velocity, and depth in (7), (8), and (9), in which the independent variable is x/D_i. If the solutions are plotted vs. x/L_e instead of x/D_i, they become universal in form as shown in Figure 4. The terms involving only B_1, B_2, and x^o in (7), (8), and (9) can be shown to reduce to functions of x/L_e and L/L_e. The dependence on Ra_m and the temperature profile shape is embedded in L_e such that specifying L/L_e establishes the complete solution for dimensionless temperature and velocity in Figure 4. The solution for the dimensionless depth in Figure 4 further requires the value of $\Delta\rho_o/\rho_o$ as can be observed from (9). Although $\Delta\rho/\rho_o$ can be determined from $(T_i - T_o)$, the relation between θ_o and L/L_e is insufficient to obtain $(T_i - T_o)$. The value of $(T_i - T_e)$ is also needed because of the nondimensionalization inherent in the definition of
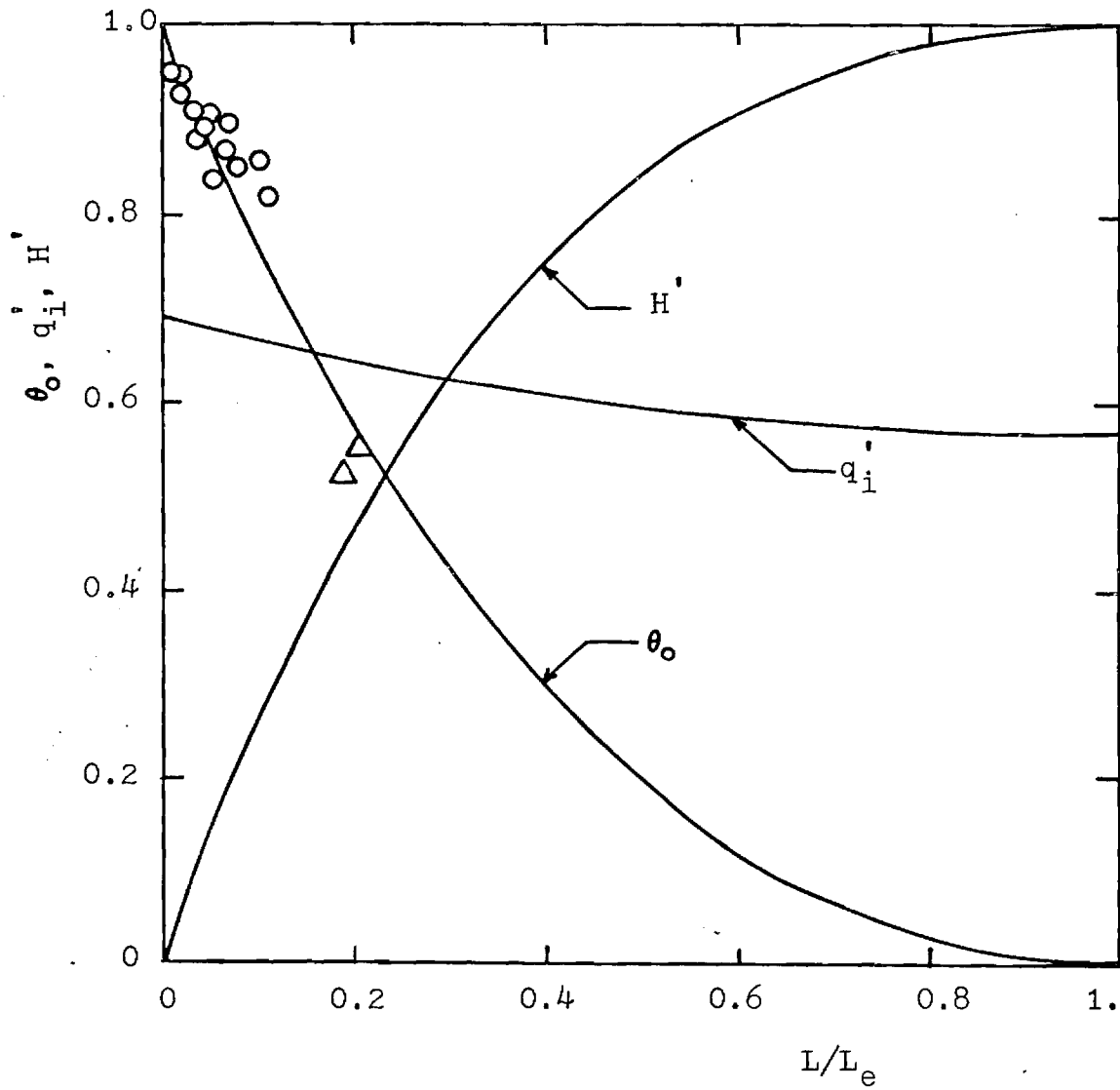
Figure 3. – Closed-Form Solutions and Experimental Results
for Dimensionless End Temperature, θ_o, Heat Loss
Rate, H', and Entrance Discharge, q'.
O – Experimental Results, Brocard et al., 1977.
△ – Experimental Results, Sturm, 1976.

Table 1 - Solution Profile Constants and Velocity Functions for $f_T(\eta) = \eta^m$

m	C_1	C_2	C_3	C_4	$f_u(\eta)$	C_0
1	576	0.275	7.20	1.60	$-\dfrac{\eta^4}{24} + \dfrac{9\eta^2}{80} - \dfrac{7\eta}{120}$	48
2	800	0.217	6.67	1.50	$-\dfrac{\eta^5}{60} + \dfrac{7\eta^2}{120} - \dfrac{\eta}{30}$	40
3	1200	0.179	7.14	1.57	$-\dfrac{\eta^6}{120} + \dfrac{3\eta^2}{84} - \dfrac{3\eta}{140}$	40
4	1764	0.152	7.88	1.68	$-\dfrac{\eta^7}{210} + \dfrac{27\eta^2}{1120} - \dfrac{5\eta}{336}$	42
5	2509	0.132	8.71	1.82	$-\dfrac{\eta^8}{336} + \dfrac{35\eta^2}{2016} - \dfrac{11\eta}{1008}$	45
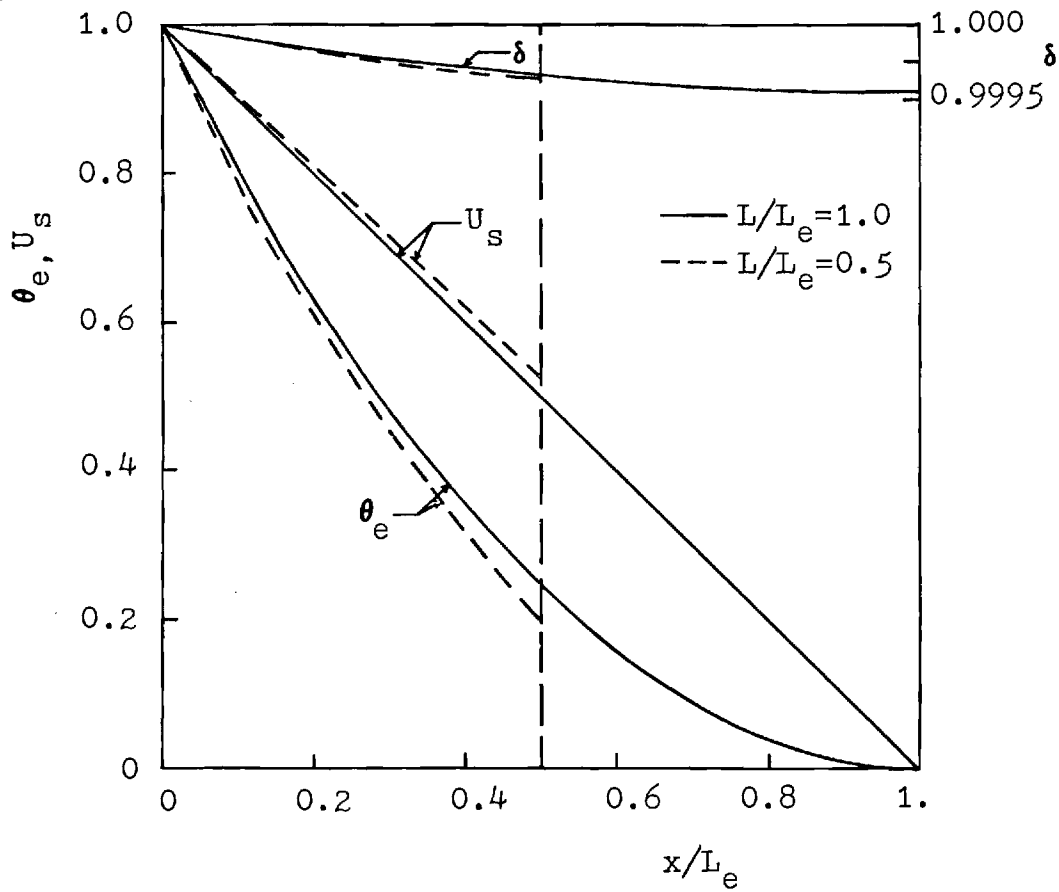
Figure 4. — Closed-Form Solutions for Longitudinal Distribution of Dimensionless Velocity, U_s, Depth, δ, and Surface Temperature, θ_e, for Equilibrium Length and Finite Length Sidearms.

θ_o. For the nondimensional depth solution, then, $(T_i - T_e)$ must be specified in addition to L/L_e. This does not decrease the generality of the solution because $(T_i - T_e)$ must also be known to calculate Ra_m and hence L/L_e. The equilibrium temperature, T_e, depends only on meteorological conditions, while T_i is the surface temperature at the entrance of the channel and must be specified.

The solutions for $L/L_e = 1.0$ and 0.5 are compared in Figure 4. As the channel length is decreased while holding constant all other variables, the velocity at $x=0$ increases due to reduced overall friction in spite of the decrease in the hydrostatic force as T_o increases. Simultaneously, the horizontal temperature gradient at $x=0$ becomes larger negatively so that heat conservation is satisfied; the net heat flux into the channel must equal the total heat flux from the water surface at steady state. The boundary values T_o and u_{si} adjust themselves as the channel length decreases such that both the thermal energy and momentum equations are satisfied.

The solutions shown in Figure 4 are affected by the choice of temperature profile shape only through a change in equilibrium length L_e. It was shown in Figure 2 that as the degree n of the temperature profile polynomial increases, the resulting velocity polynomial, $f_u(\eta)$, decreases in magnitude over the full depth of flow. For a channel of given length and specified value of Ra_m, the surface velocity at $x=0$, u_{si}, becomes smaller as n increases because of the decrease in the buoyant force arising from the hydrostatic pressure force difference between the entrance and the dead end of the channel. Consequently, there is a decrease in the net heat transported into the channel and a greater surface temperature drop, $(T_i - T_o)$, over the full

length of the dead end channel. These effects are reflected in Figure 4 by a decrease in the equilibrium length.

The depth decreases toward the dead end of the channel as shown in Figure 4 in order to drive the inflow current as postulated in §2.2. Although the depth change is very small, it makes a significant contribution to the horizontal pressure gradient and thus to the magnitude of the velocity at any x. As the contribution of the horizontal temperature gradient to the pressure gradient goes to zero for x/L_e approaching 1.0, so also does the contribution of the depth gradient. For a channel of given length $L < L_e$, the depth will increase with x as the surface temperature T_s approaches T_o so that the velocity can be forced to zero as the dead end is reached. This depth increase will occur over a relatively short reach of the channel near the dead end. Over this short reach, the formulation and solutions presented herein are not applicable.

The solutions for θ_o, q_i', and H' in Figure 3 indicate how the boundary conditions and heat loss vary with the ratio L/L_e. The solutions themselves are practically insensitive to the temperature profile shape (see Table 1 for variation in C_4 which appears in (13)), but the value of L_e is quite dependent on $f_T(\eta)$. The heat-loss rate increases very rapidly with γ. Approximately 83 percent of the maximum possible rate of heat loss and 80 percent of the maximum surface temperature drop occur in a channel which has a length that is only 50 percent of the equilibrium length. As a result, the value of q_i' changes very little for $L/L_e > 0.5$. For $L/L_e < 0.5$, q_i' increases gradually with a decrease in channel length as discussed previously. The curve for θ_o in Figure 3 should not be interpreted as the rate at which the surface temperature decreases with x for a given channel length, but rather as the locus of boundary values, T_o, for channels of variable length.

The concept of an equilibrium length was developed because of the
generality it provides in the presentation of the solutions in Figures 3
and 4. It is not intended to obscure the controlling dimensionless para-
meter of the free convection in the dead-end channel. This parameter is
the modified Rayleigh number, Ra_m, which emphasizes the dominance of the
buoyancy and viscous forces and the importance of surface heat transfer
in a central region of the dead-end channel for which $L/D >> 1$. Decreasing
the fluid viscosity in a channel of given length, for example, increases
Ra_m and L_e/D and as a result, the inflow velocity increases while the sur-
face temperature drop, $(T_i - T_o)$, decreases. On the other hand, increasing the
surface heat transfer coefficient K decreases Ra_m, and $(T_i - T_o)$ increases.
Thus, the modified Rayleigh number measures not only the relative impor-
tance of buoyancy and viscous forces but also the rate at which the driv-
ing buoyancy force is being lost by surface heat transfer to the atmosphere.

The limitations of neglecting the inertia terms in (1) can be examined
in light of the closed-form solution which has been obtained. If the closed-
form solution is utilized to provide a first-order estimate of the magnitude
of the inertia terms, their relative importance when compared with the buoy-
ancy and viscous terms in (1) can be assessed. The ratio of inertia to
buoyancy forces is given by the following definition of densimetric Froude
number, F:

$$F^2 = \frac{u_{si}(\Delta u_s/L)}{g(\frac{dD}{dx})_i} \qquad (16)$$

in which u_{si} is the surface velocity at $x=0$; Δu_s is the decrease in surface
velocity from $x=0$ to the end region (assumed to be very short) where $x=L$;
and $(dD/dx)_i$ is the slope of the free surface at $x=0$. The evaluation of

F^2 has been chosen at a point where the inertia forces can be expected to have their maximum value. The buoyancy force at the free surface, where the inertia terms are evaluated, is contributed solely by the slope of the free surface that is necessary to balance the effect of the horizontal density gradient integrated over the depth.

If u_{si}, Δu_s, and $(dD/dx)_i$ are evaluated by the closed-form solution, the following expression is obtained for F^2:

$$F^2 = \frac{1}{Pr_m} \left(\frac{C_3{}^2}{3C_1 C_2} \right) \tag{17}$$

in which C_1, C_2, and C_3 are profile constants given in Table 1, and Pr_m is a modified Prandtl number defined by $\mu c_p / KD$, where K is the local coefficient of surface heat transfer; D is the depth; c_p is spceific heat; and μ is absolute viscosity. If the inertia terms are indeed small, then $F^2 \ll 1$ which requires that $Pr_m \gg 8 \times 10^{-2}$. The choice of m=3,4, or 5 in Table 1 gives virtually the same limiting value of Pr_m. Using typical values of $K=2 \times 10^{-3}$ w/cm^2-$^\circ$C and D=20 cm for laboratory conditions with water as the fluid, Pr_m has a value of approximately 1.0, which is at least one order of magnitude larger than the limit at which the inertia terms must be considered. Thus, it seems that for Pr_m sufficiently large, it is possible to neglect the inertia terms in (1), at least as a first approximation.

On the other hand, the convective terms in the thermal energy equation, (3), cannot be neglected. The heat that is lost through the free surface must be balanced by the net logitudinal convection of heat. The vertical heat diffusion terms, which supply the heat to the free surface, must be much larger than the horizontal diffusion terms if L/D >>1 and, as a result, must be of the same order as the longitudinal convection terms.

2.5 Comparison of Solution with Experimental Results

For the purpose of comparison with the closed-form solution, the experimental results of Brocard et al. (1977) as well as those of the author (Sturm, 1976) are considered. The experiments by Brocard et al. (1977) were conducted in a 10.7-m long flume with a head tank which was wider than the flume and into which heated water was introduced through a radial diffuser. An equal discharge of water was withdrawn through a multiport outlet device in the head tank. The resulting stratified temperature profile at the entrance to the channel produced a gravity circulation in the channel similar to that for the author's experiments in which an electrical resistance heating rod served as the heat source.

The distribution of surface temperature along the channel obtained from the closed-form solution is compared with the author's experimental run B and with experimental run 14 of Brocard et al. (1975) in Figure 5. For both runs, the temperature profile polynomial has been assumed to be $f_T(\eta) = \eta^5$ because the temperature profiles were similar in shape. The height of the inflection point in the temperature profile (measured above the channel bottom) was 0.75 times the depth for run B and 0.70 times the depth for run 14. Only the downstream 13 m of the channel in run B are included in the central region due to the vertical currents that occurred in the region of flow establishment. It can be seen in Figure 5 that the agreement with the closed-form solution is much better for run 14 than for run B. A portion of the discrepancy in run B may be attributed to a surface heat-loss relationship which was highly nonlinear.
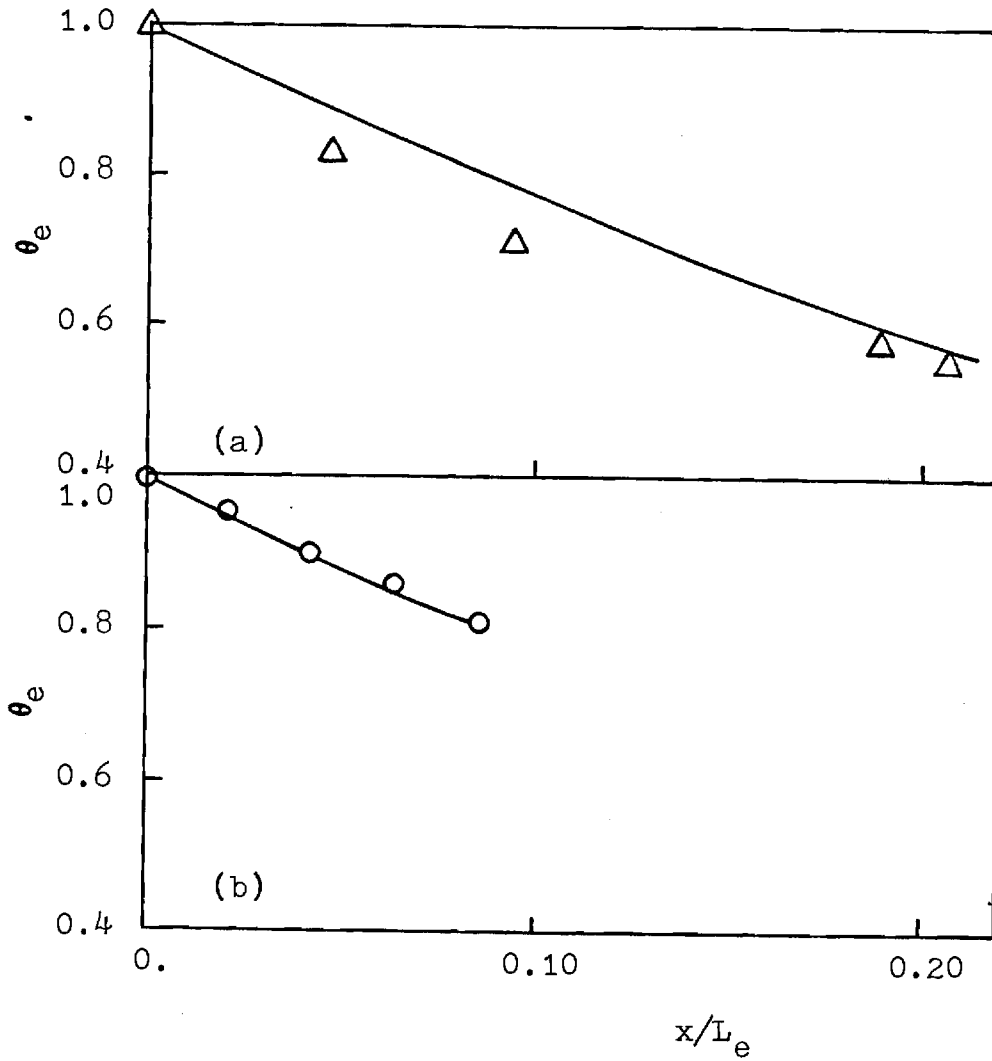
Figure 5. – Comparison of Closed-Form Solution with
Experimental Results for Longitudinal
Distribution of Dimensionless Surface
Temperature, θ_e.
O – Experimental Results, Brocard et al., 1975.
Δ – Experimental Results, Sturm, 1976.

In Figure 3 the closed-form solution for θ_o is compared with

the author's data and selected data of Brocard et al. for which the

height of the point of inflection in the temperature profiles

measured from the channel bottom varied from 0.55 to 0.65 times the

depth. This allowed each data set to be plotted according to a single

temperature profile shape, which was chosen to be $f_T(\eta) = \eta^4$ for the

selected data of Brocard et al. and $f_T(\eta) = \eta^5$ for the author's data.

The influence of the chosen temperature profile shape appears in the

value of L_e and hence in the plotting position of the experimental

data along the horizontal axis in Figure 3. The solution curves for

θ_o and H' are unaffected by temperature profile shape.

The choice of profile constants made for each set of experimental

data seems to have produced reasonable agreement between the experimental

and calculated values of θ_o in Figure 3. The values of K needed in the

calculation of Ra_m were determined as $K = - \phi_{ni}/(T_i - T_e)$, where ϕ_{ni}

is the rate of surface heat loss per unit area at x = 0. Empirical

relations for ϕ_{ni} are necessary to determine K, and those relations

suggested by Brocard et al. were used for their data in Figure 3.

For the author's data, the relation for evaporative heat flux was

altered slightly to satisfy a heat balance for the flume.

2.6 Summary

It has been shown in this chapter that a closed-form solution of

the coupled equations of motion and thermal energy reproduces the

essential aspects of laboratory results for thermally-induced gravity

currents in the laminar regime. The governing dimensionless parameter

of the problem is a modified Rayleigh number, which was shown to determine not only the solutions for temperature, velocity, and depth, but also the initially unknown velocity and temperature boundary conditions. The results of the closed-form solution are limited by the assumption of laminar flow and the relatively simple shapes chosen for the temperature profiles, but this line of investigation was found to be very fruitful in determining the interaction of wind-driven and gravity currents as discussed in the following chapter.

3. WIND STRESS INTERACTION WITH GRAVITY CURRENTS

3.1 Introduction

The closed-form solution for laminar gravity currents given in the
previous chapter forms a convenient starting point for evaluation of the
interaction of an imposed wind stress at the water surface with a
gravitational circulation. If the wind stress is assumed to be steady,
uniform, and directed toward the dead end of a cooling lake sidearm,
two effects will occur. First, wind will increase the forced convection
component of evaporative heat loss from the water surface. This in-
creases the driving buoyant force of the gravitational circulation, and
the overall surface water temperature drop from the sidearm entrance to
its dead end will be greater. Second, as the intensity of the wind
stress increases, wind-driven surface currents can be expected to
develop. These currents would tend to carry heated water into the
sidearm from the main body of the cooling lake, and could conceivably
become so large that the entire water surface temperature in the side-
arm is nearly equal to the surface temperature in the lake at the
entrance of the sidearm. In this case, the sidearm surface area is
equally as effective as the surface area of the main body of the lake
in transferring excess heat to the atmosphere. In this chapter, these
two effects of a constant wind stress on gravity currents in a cooling
lake are investigated by an extension of the formulation and closed-
form solution for laminar gravity currents as given in the previous
chapter.

Some previous research has dealt with the analysis of wind-driven currents alone. Liggett and Hadjitheordorou (1969) and Lee and Liggett (1970) present solutions to the governing equations of motion for three-dimensional wind-driven circulations in shallow, homogeneous lakes and in stratified lakes for a steady, uniform wind. With the exception of the inclusion of Coriolis forces, the governing equations used in these studies are similar to those developed for laminar gravitational circulations presented in the previous chapter. The inertia forces and the horizontal diffusion of momentum in the equations of motion are neglected, and the vertical pressure distribution is assumed to be hydrostatic. Horizontal gradients in density, however, are not considered. A constant eddy viscosity is assumed to exist throughout a homogeneous lake, and different constant values are assumed in each of two layers for a stratified lake.

Banks (1975) has solved the equations of motion for wind-driven circulation in the vertical plane only with the Coriolis force neglected. He obtains a velocity distribution similar to what would be expected for a combined Couette-Poiseuille laminar flow between parallel plates. A return flow opposite in direction to the wind exists below the surface wind-driven current with the point of zero velocity crossover at a distance of 2/3 the depth measured upward from the bottom plate.

Wind-driven currents have been studied in laboratory experiments by Wu (1973), Baines and Knapp (1965), and Hidy and Plate (1966). Wu's experiment was concerned primarily with turbulent entrainment by a wind-driven current in a stratified flow. He showed that the change in potential energy of the mixing layer due to entrainment is proportional

to the rate of work done by the wind on interfacial mixing. This result will be discussed more thoroughly in a succeeding chapter of this report. The experiments by Baines and Knapp (1965) in a homogeneous fluid clearly showed the return flow expected from a Couette Poiseuille flow analysis but found that velocity concentrations like jets occurred close to the surface and the bed. They attributed this behavior to the existence of large eddies in the central region of the flow which were inhibited by viscosity near the surface and bed. The experiments by Hidy and Plate (1966) were concerned primarily with wave generation by wind in a laboratory channel, but they do present an experimental relation for determining the wind shear stress for drift currents. This relation will be referred to again later in this chapter.

3.2 Formulation and Solution

The formulation of the problem is identical to that in the previous chapter with the exception of the boundary condition at the free surface where the shear stress, τ_s, becomes:

$$\tau_s = \mu \frac{du}{dy} = C_D \rho_a V_w^2 \tag{18}$$

in which C_D is a coefficient of drag; ρ_a is the density of air; and V_w is the wind speed. Neglecting the inertia terms in the horizontal momentum equation and assuming a hydrostatic pressure distribution in the vertical direction are assumptions consistent with the formulation for laminar gravity currents alone, as justified in the

previous chapter, and with previous research on wind-driven currents. The problem to be solved then is the combination of a laminar gravitational circulation in a dead-end channel as shown in Figure 1 with the wind-driven circulation due to a nonzero surface shear stress imposed at the free surface toward the dead end.

Following the development of Equation (5) from the equations of motion for gravitational circulation alone, the addition of the wind stress boundary condition given by Equation (18) results in:

$$u = \frac{\alpha g D^3}{\mu} \frac{d(T_s - T_o)}{dx} f_u(\eta) + \frac{\tau_s D}{\mu} f_w(\eta) \qquad (19)$$

in which $f_w(\eta) = (3/4)\eta^2 - (1/2)\eta$. The additional velocity polynomial in (19) given by $f_w(\eta)$ has a zero at two-thirds the depth from the bottom of the channel. It does not depend on the chosen temperature profile shape as does $f_u(\eta)$. The value of τ_s is taken to be a known constant in (19) and in the following development but will be related to the wind velocity subsequently when the solution results are applied.

The expression for the velocity distribution given by (19) is substituted into the thermal energy equation, (3), as before, and a new ordinary differential equation is the result:

$$\theta_s \frac{d^2\theta_s}{dx^{\circ 2}} + \left(\frac{d\theta_s}{dx^{\circ}}\right)^2 - \left(\frac{C_1}{C_0} \frac{S_w}{\Delta\rho_o/\rho_o}\right)\frac{d\theta_s}{dx^{\circ}} - \left(3\frac{C_1}{C_0} \frac{S_w^2}{\Delta\rho_o/\rho_o} + B_1\right)\theta_s - \frac{B_1\theta_o}{(1 - \theta_o)} = 0$$

$$(20)$$

In Equation (20), which has been cast in dimensionless form, $S_w = \tau_s/\gamma D$; $\Delta\rho_o = \rho(T_o)-\rho(T_i)$; $\rho_o = \rho(T_o)$; and C_0 is a profile constant given by:

$$C_0 = \left[\int_0^1 f_w(\eta)f_T(\eta)\,d\eta \right]^{-1} \tag{21}$$

Values of C_0 are given in Table 1. Two additional terms in Equation (20) in comparison to Equation (6) are apparent and are the result of the wind stress boundary condition. Unfortunately, the addition of the third term on the left hand side of Equation (20) precludes the closed-form solution that was obtained for gravitational circulation alone.

Equation (20) was solved numerically using the Runge-Kutta method. The solution was found to be quite stable and reduced to the closed-form solution for $S_w = 0$. The solution is started at the closed end of the sidearm by specifying Ra_m, S_w, (T_i-T_e), and Θ_o. From the latter two variables, $\Delta\rho_o/\rho_o$ can be calculated, and then all parameters in Equation (20) are known. The solution proceeds in steps toward the open end of the sidearm until $\theta_s = 1.0$, and the length of sidearm required for the specified Θ_o becomes known. At each step of the solution, θ_s and $d\theta_s/dx$ are determined by the Runge-Kutta method.

From the solution for $\theta_s(x)$, it is possible to determine the solutions for velocity and depth for all x. Equation (19) is solved for the surface velocity u_s by setting $\eta = 1.0$. In nondimensional

form, we have:

$$\frac{u_s}{k/\rho c_p} = - Ra_m(1 - \theta_o) \ f_u(1) \frac{d\theta_s}{dx^o} + \frac{S_w Ra_m(1 - \theta_o)f_w(1)}{\Delta\rho_o/\rho_o} \qquad (22)$$

It is of interest to note that the contribution of the wind-driven current to the surface velocity in the second term on the right hand side of (22) is a constant, while the contribution of the density (temperature) gradient varies with x. The solution for the depth variation with x is obtained from the integration of Equation (4) with $\partial u/\partial y = \tau_s/\mu$ at y=D and from the continuity condition: $\int_0^1 u d\eta = 0$. The result for the depth gradient in nondimensional form, from which the depth can be determined, is given by:

$$\frac{d\delta}{dx^o} = C_2 \frac{\Delta\rho_o}{\rho_o} \frac{d\theta_s}{dx^o} + \frac{3}{2}S_w \qquad (23)$$

in which $\delta = D/D_i$; D_i is a reference depth; and C_2 is a profile constant for which values are given in Table 1.

Finally, the rate of surface heat loss from the dead-end channel is determined from:

$$H_L = K \ b \int_0^L (T_s - T_e) \ dx \qquad (24)$$

In nondimensional terms, Equation (24) can be written as:

$$\frac{H_L}{KbL(T_i - T_e)} = \frac{\int_0^{L/D} \theta_e dx^o}{L/D} \qquad (25)$$

in which $\Theta_e = (T_s-T_e)/(T_i-T_e)$ and is related directly to Θ_s by

$$\Theta_e = \Theta_s(1-\Theta_o) + \Theta_o \tag{26}$$

The left hand side of Equation (25) is the ratio of the actual surface heat loss rate to that which would prevail if the surface temperature were equal to T_i for all x in a channel of length L and width b. The integral in (25) was evaluated by the trapezoidal rule from the Runge-Kutta solution for $\Theta_e(x)$.

3.3   Results and Discussion

Because the introduction of equilibrium length as a reference length conveniently nondimensionalized the solutions for gravity currents alone, it is also useful to consider the effect on the equilibrium length of adding a surface wind stress. Because of the additional dimensionless parameters which appear in Equation (20), it can be inferred that:

$$\frac{L_e}{D_i} = f\left(Ra_m, \frac{\Delta\rho_e}{\rho_e}, S_w, C_1\right) \tag{27}$$

in which L_e is the equilibrium length and C_1 is a temperature profile constant as before, and $\Delta\rho_e = \rho(T_e) - \rho(T_i)$. Note that for the equilibrium case, $T_o = T_e$ and $\Delta\rho_o = \Delta\rho_e$. In comparison with Equation (11), the equilibrium length is now a function of two additional parameters: the density deficit ratio and the dimensionless wind shear stress.

Numerical results for equilibrium length are shown in Figure 6

for the temperature profile shape given by $f_T(\eta) = \eta^4$ and for various

values of S_w and $\Delta\rho_e/\rho_e$. Although it is not possible to increase

the windspeed and S_w without also decreasing the Rayleigh number

because of increased surface heat transfer, it is apparent from

Fig. 6 and Equation (20) that the equilibrium length generally

increases with increases in windspeed due to increased horizontal

advection by the wind-driven current considered alone. Decreasing

the density deficit ratio, $\Delta\rho_e/\rho_e$, results in reducing the relative

influence of horizontal advection by the gravity current compared to

that by the wind-driven current, and so the equilibrium length in-

creases.

By analyzing a large number of results for equilibrium length,

it was observed that the results could be presented more simply as

shown in Figure 7, in which the independent variable is $Ra_m^{1/2}$

$S_w/(\Delta\rho_e/\rho_e)$. The ratio of the shear stress parameter to the density

deficit appears in the third term in Equation (20) and the $Ra_m^{1/2}$

dependence is the same as that found for equilibrium length in the

case of a gravity current alone. For small values of the independent

variable in Figure 7, the curve approaches a slope of minus one, and

the dependence on $Ra_m^{1/2}$ alone for zero wind shear is recovered. As

the wind shear becomes large, the curve becomes horizontal and the

equilibrium length is proportional to $Ra_m S_w/(\Delta\rho_e/\rho_e)$.

In Figures 8 and 9, typical solutions for Θ_e, δ, and U_s/U_{si} are

shown as a function of x/L_e in analogy to the presentation of solutions

for a gravity current alone in Figure 4. The solutions in Figure 8

are for $\Delta\rho_e/\rho_e = 3 \times 10^{-3}$, and in Figure 9 are for $\Delta\rho_e/\rho_e = 1.5 \times 10^{-3}$.
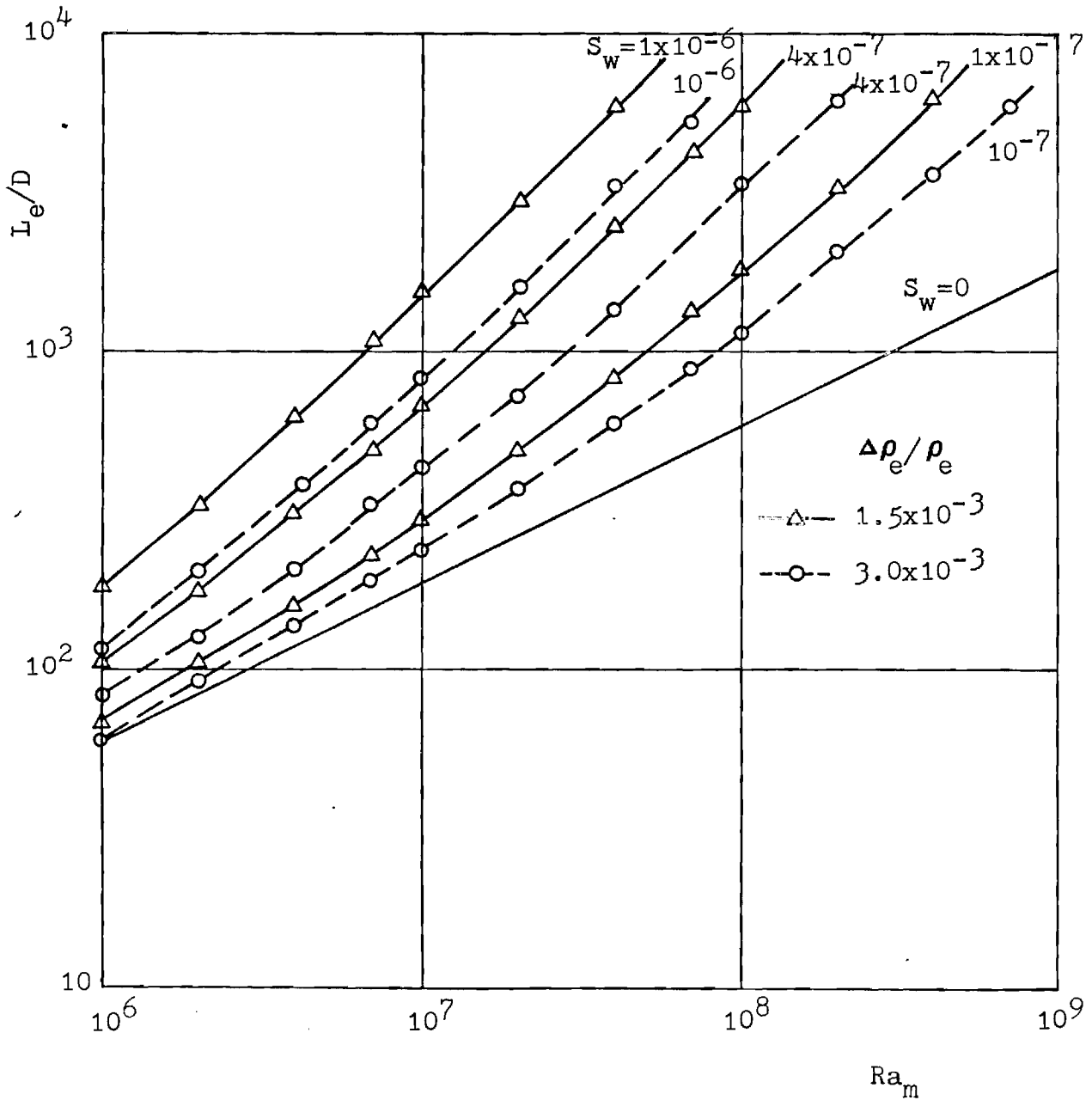
Figure 6. – Equilibrium Length, L_e, for Combined Gravity and Wind Driven Circulation $(f_T(\eta)=\eta^4)$.
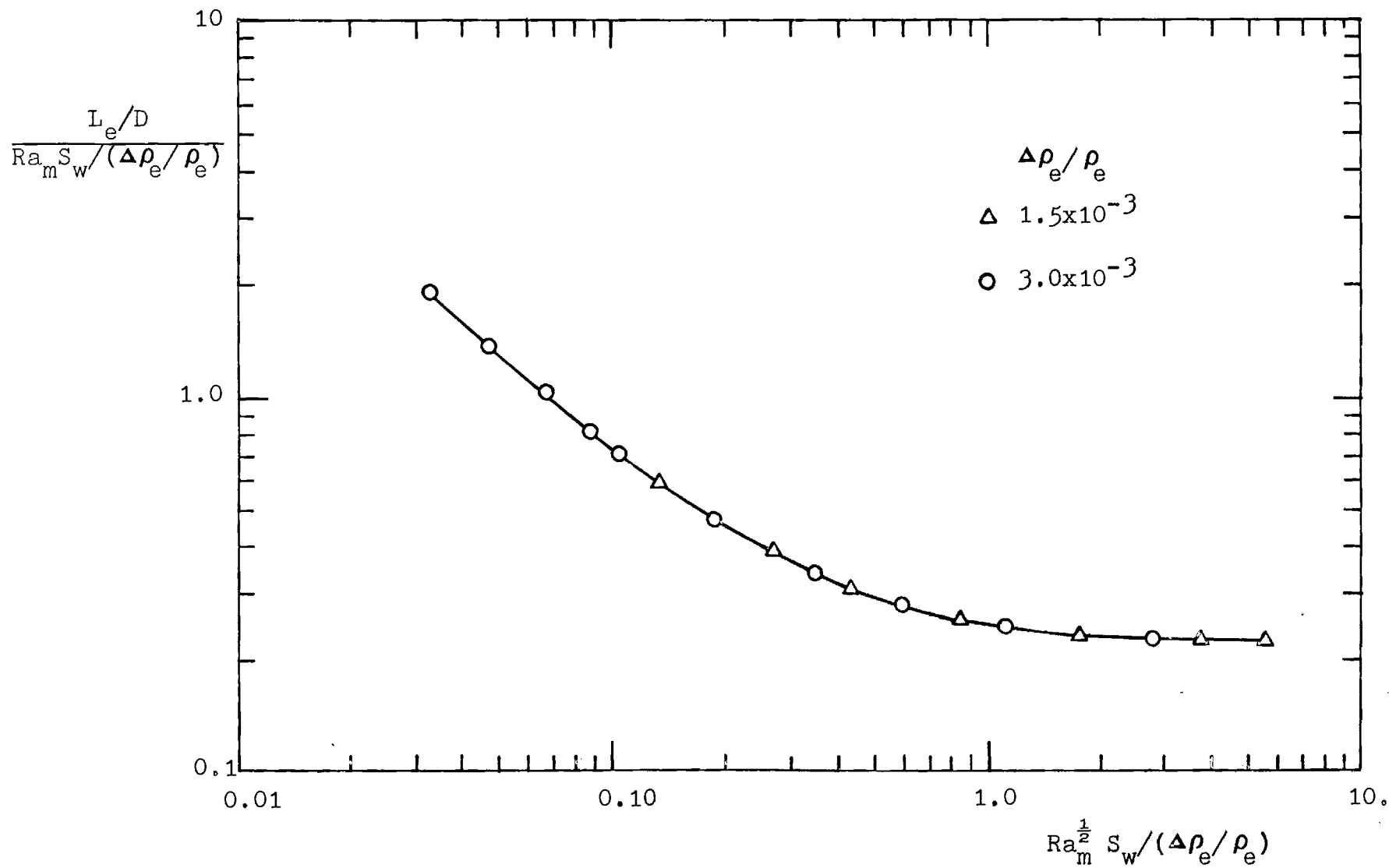
Figure 7. – Consolidation of Results for Equilibrium Length in Combined Gravity and Wind Driven Circulation $(f_T(\eta)=\eta^4)$.

In both Figures 8 and 9, $f_T(\eta) = \eta^4$ and $Ra_m^{1/2} S_w = 1 \times 10^{-3}$. The same dimensionless solutions are produced for different values of Ra_m and S_w as long as $Ra_m^{1/2} S_w$ is held constant. By comparing Figures 4 and 8, the effect of the wind stress on gravitational circulation is apparent. The surface velocity approaches the constant value associated with the wind-driven current as x approaches L_e. In addition, the surface temperature decreases more rapidly with respect to x/L_e as a result of wind shear, but it must be recalled that the wind shear also increases the equilibrium length. As x/L_e approaches one, the curve for dimensionless depth, δ, indicates that wind setup is occurring as expected. Also shown in Figure 8 are the solutions for a channel of specified length, $L/L_e = 0.2$. The solutions for velocity and depth are practically the same as for the equilibrium-length channel, but the surface temperature decreases more rapidly for the channel of specified length. In Figure 9, $\Delta\rho_e/\rho_e$ has been decreased to 1.5×10^{-3}. This seems to increase the relative influence of the wind-driven current compared to the gravity current.

As in the case of gravitational circulation alone, the boundary condition of $\Theta_s = \Theta_o$ at x = L is initially unknown, but it can be determined from the numerical procedure developed herein for a combined gravity and wind-driven circulation. The numerical results for Θ_o are presented in Figure 10 as a function of L/L_e. The necessary parameters are $Ra_m^{1/2} S_w$ and $\Delta\rho_e/\rho_e$ as in Figures 8 and 9. In comparison with the curve in Figure 3 for θ_o, it is apparent that the wind shear reduces θ_o at similar values of L/L_e although the wind shear also increases L_e. The curves in
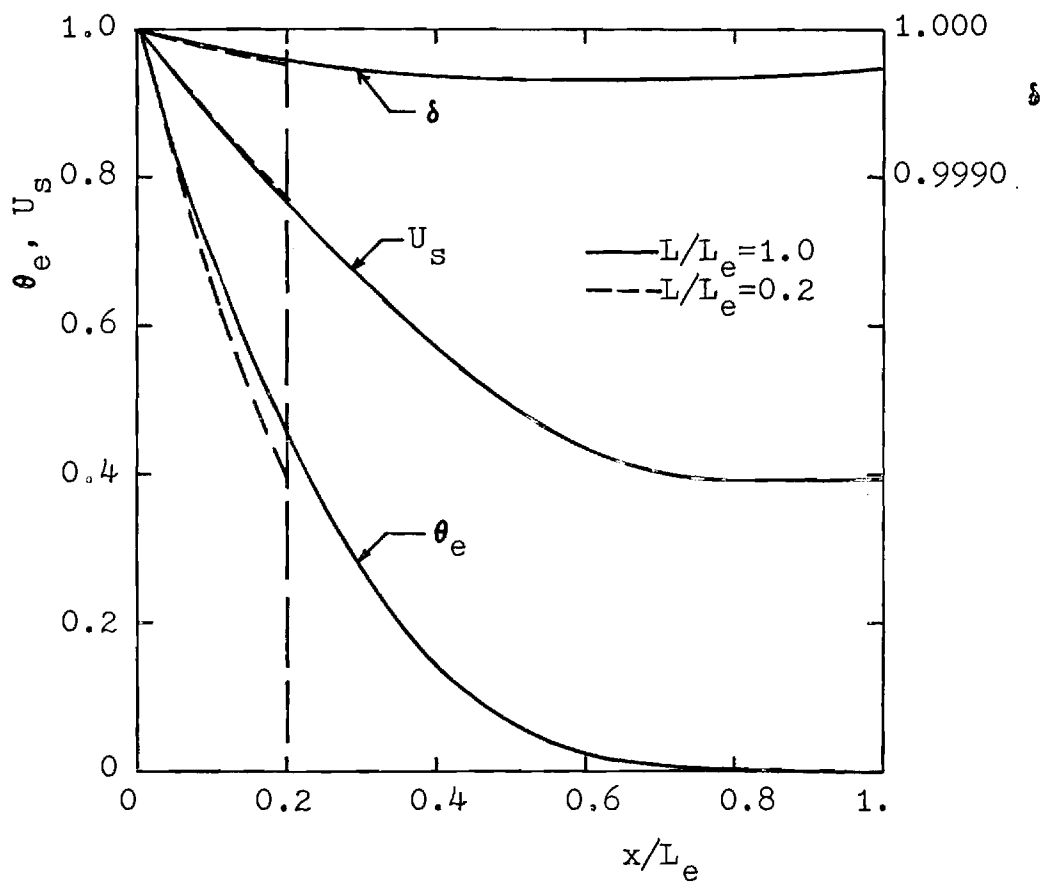
Figure 8. – Numerical Solutions for Longitudinal
Distribution of Dimensionless Velocity,
U_s, Depth, δ, and Surface Temperature,
θ_e ($\Delta\rho_e/\rho_e = 3.0 \times 10^{-3}$; $Ra_m^{1/2} S_w = 1 \times 10^{-3}$).
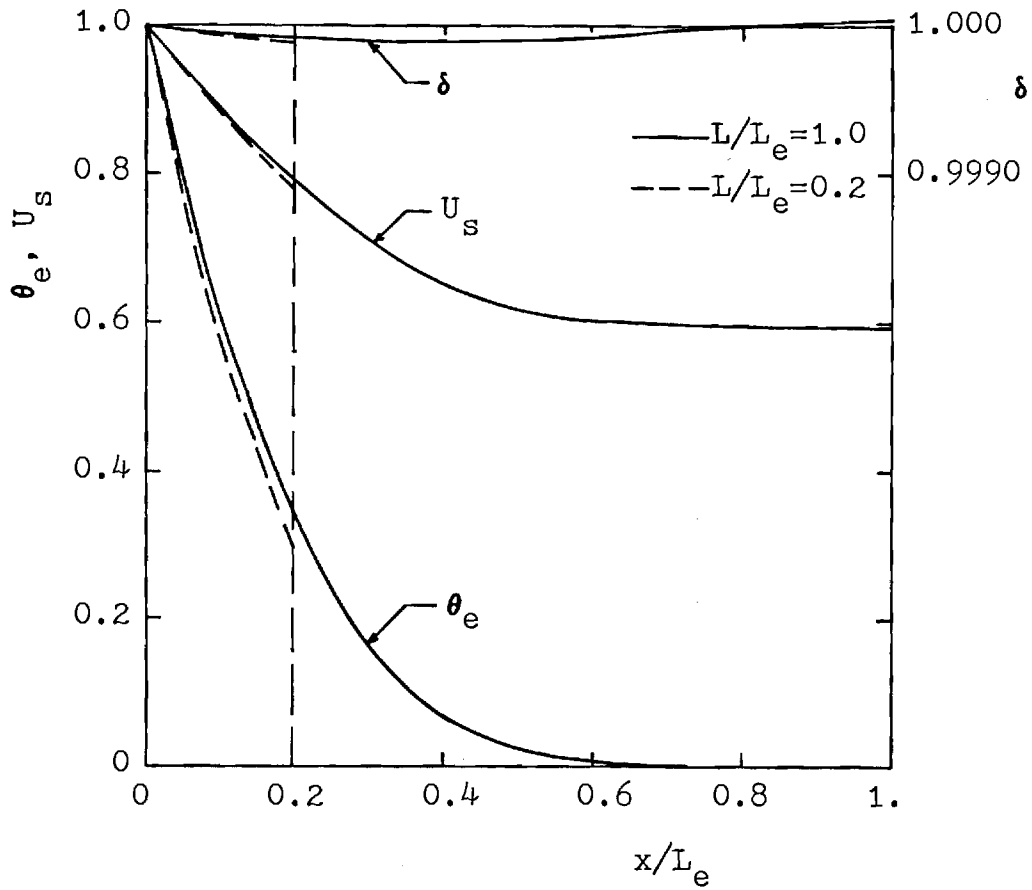
Figure 9. – Numerical Solutions for Longitudinal
Distribution of Dimensionless Velocity,
U_s, Depth, δ, and Surface Temperature,
$\theta_e (\Delta\rho_e/\rho_e = 1.5 \times 10^{-3}; \text{Ra}_m^{1/2} S_w = 1 \times 10^{-3})$.
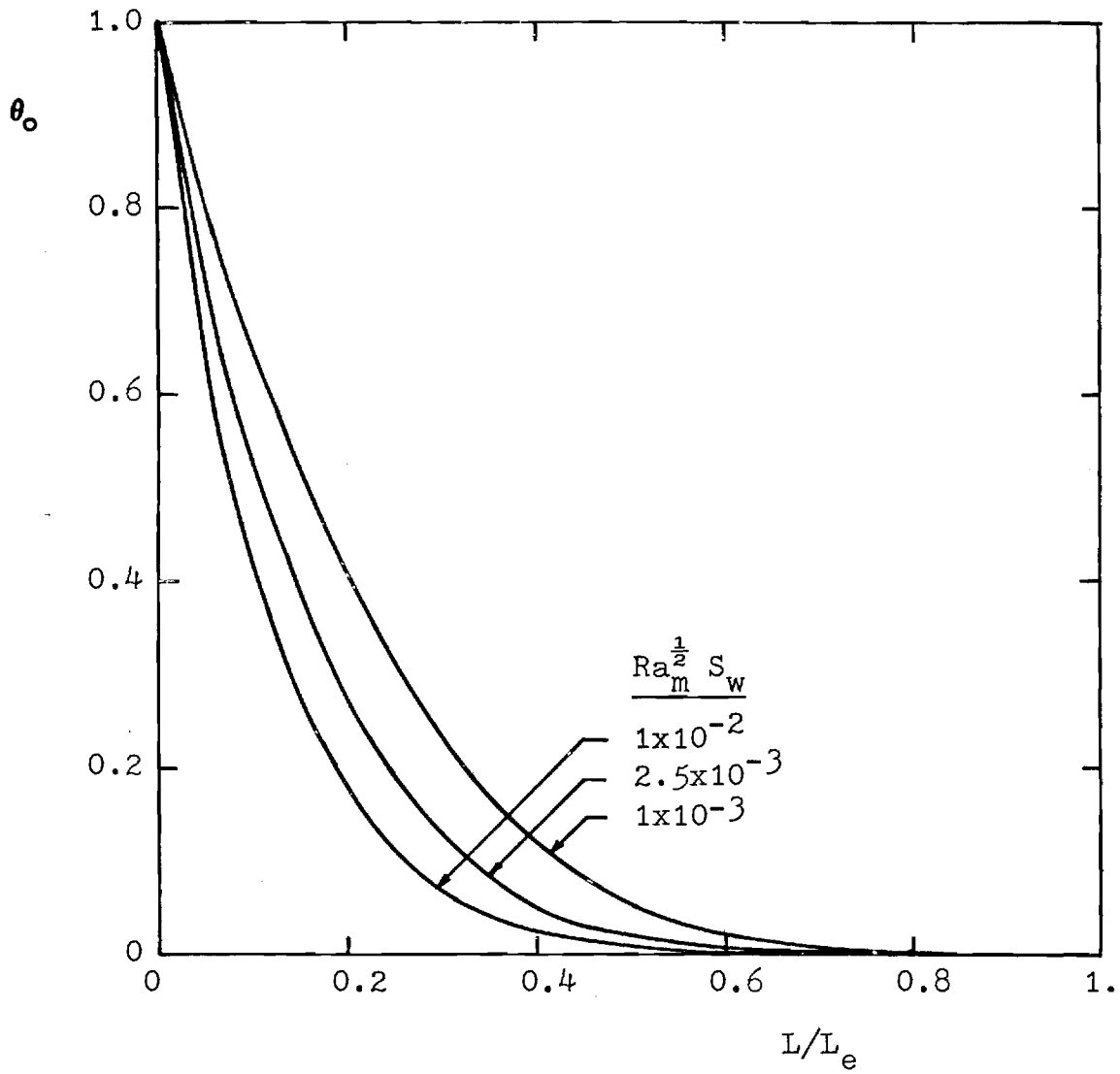
Figure 10. – Numerical Solutions for Dimensionless End
Temperature, θ_o ($\Delta\rho_e/\rho_e$ = 3.0 x 10^{-3}).

Figure 10 are useful for determining the amount of surface temperature drop that might be expected in the channel for various wind conditions.

The numerical results presented in Figure 11 can be used to determine the total rate of heat loss from the sidearm, H_L, as a fraction of the local surface heat transfer rate evaluated for the known water surface temperature, T_i, at the sidearm entrance. The results are a function of $Ra_m^{1/2} S_w$, $\Delta\rho_e/\rho_e$, and L/L_e. The closed-form solution for a wind speed of zero is also shown in Figure 11, and it is independent of $\Delta\rho_e/\rho_e$. For very large wind speeds in a sidearm of given length, the equilibrium length becomes very large and L/L_e approaches zero. Thus, the rate of heat loss approaches that which would occur if the water temperature were everywhere equal to T_i. In the other limiting case of zero wind speed, significant heat loss still occurs due to the existence of the gravitational circulation alone.

3.4   Application of Results

The relative influence of wind speed on laminar gravity currents can be illustrated with a specific example in which the numerical results presented herein are applied. Consider a laboratory sidearm 100 ft long with a depth of 0.5 ft. Air temperature is assumed to be 75°F, and the relative humidity is taken to be 75%. The surface temperature at the sidearm entrance is maintained at a constant elevation of 20°F greater than equilibrium temperature as the wind speed is increased, and this gives a constant value of $\Delta\rho_e/\rho_e = 10^{-3}$.
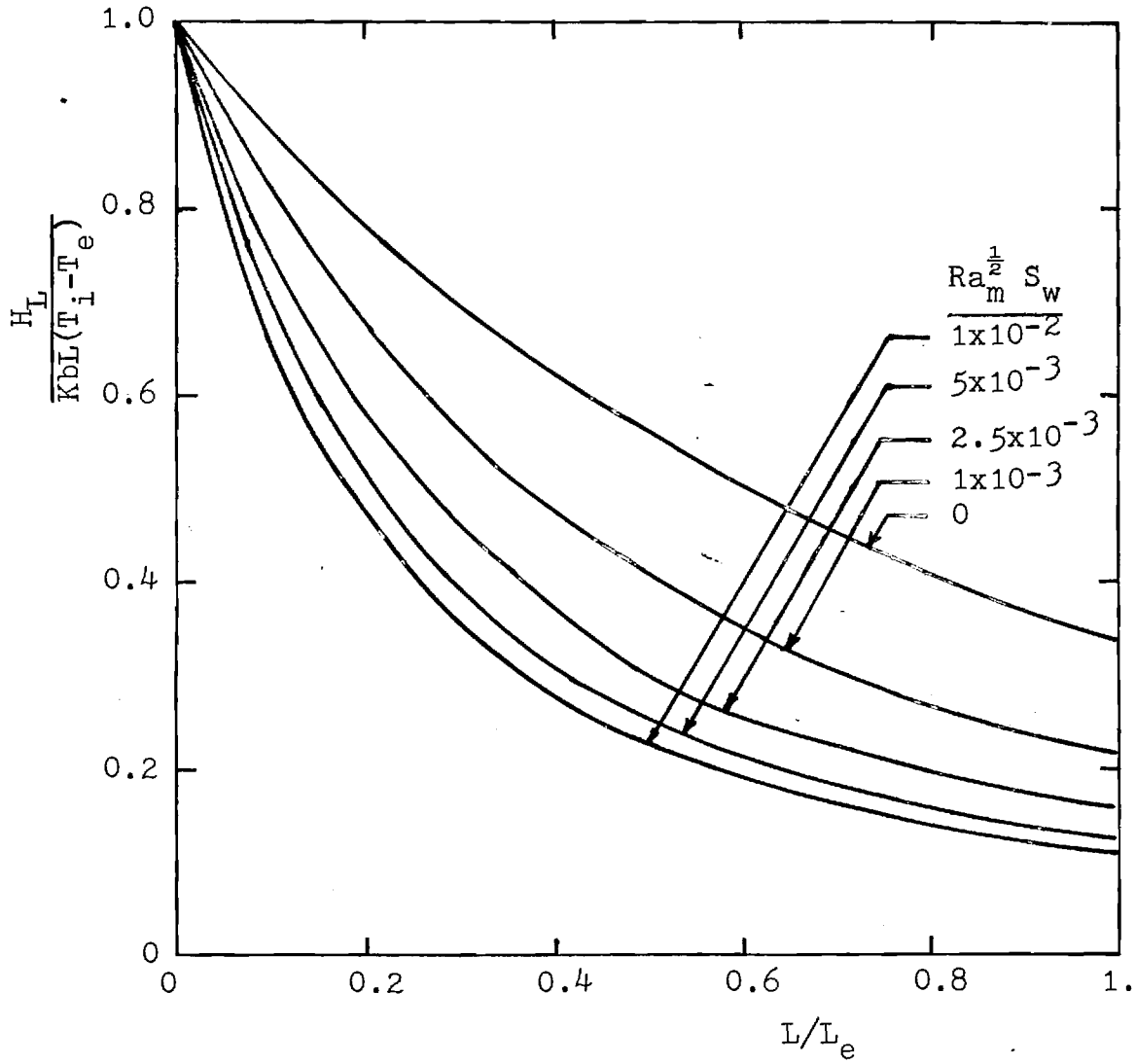
Figure 11. — Total Rate of Surface Heat Loss, H_L, from Sidearm of Length, $L(\Delta\rho_e/\rho_e = 3.0 \times 10^{-3})$.

The wind shear stress is determined from a relation presented by
Hidy and Plate (1966) for a laboratory channel:

$$\tau_s = (6.67 \times 10^{-4} \ V_w) \ \rho_a V_w^2 \tag{28}$$

where the expression inside the parentheses assumes a linear variation
between C_D and V_w with V_w in m/sec.

The surface heat loss rate is determined from the numerical
results for a series of increasing values of wind speed. The results
are shown in Table 2 and Figure 12. As the wind speed increases, the
local surface heat transfer coefficient, K, also increases and this
decreases the values of Ra_m as shown in Table 2. For given values of
Ra_m and wind shear parameter, S_w, the equilibrium length is determined
from Figure 7. Then with values of L/L_e, $Ra_m^{1/2}S_w$, and $\Delta\rho_e/\rho_e$, the
surface heat loss rate can be determined from Figure 11.

The results for surface heat loss rate in Figure 12 show that
the heat loss rate increases with wind speed slowly at first and then
increases more rapidly for larger wind speeds, eventually approaching
a linear rate of increase. This linear rate is due primarily to the
assumed linear form of the relation between evaporative heat flux and
wind speed for a given vapor pressure difference between the water
surface and air. In this region of higher wind speeds, the surface
temperature has approached its maximum value of T_i throughout the
sidearm, and the wind-driven current has overpowered the gravity
current. At small wind speeds, on the other hand, the increased
local surface heat transfer due to the wind reinforces the gravi-
tational circulation and it remains important.

Table 2. - Example Problem Results for Heat Loss Due to Combined
Gravitational and Wind Driven Circulations (D = 0.5 ft;
L = 100 ft; T_{air} = 75°F; Rel. Hum. = 75%; $T_i - T_e$ = 20°F).

V_w ft/s	T_e °F	T_i °F	$\dfrac{K}{\dfrac{BTU}{ft^2-sec-°F}}$	Ra_m	S_w	$\dfrac{L}{L_e}$	$\dfrac{H_L}{KbL(T_i-T_e)}$
0	70.12	90.12	1.10×10^{-3}	1.48×10^8	0	.282	.710
1.0	70.0	90.00	1.22×10^{-3}	1.33×10^8	1.5×10^{-8}	.264	.710
1.5	69.95	89.95	1.28×10^{-3}	1.27×10^8	5.06×10^{-8}	.201	.721
2.0	69.90	89.90	1.34×10^{-3}	1.21×10^8	1.20×10^{-7}	.132	.744
3.0	69.82	89.82	1.46×10^{-3}	1.11×10^8	4.05×10^{-7}	.0556	.821
4.0	69.76	89.76	1.58×10^{-3}	1.03×10^8	9.59×10^{-7}	.0270	.891
5.0	69.70	89.70	1.70×10^{-3}	9.55×10^7	1.87×10^{-6}	.0149	.934
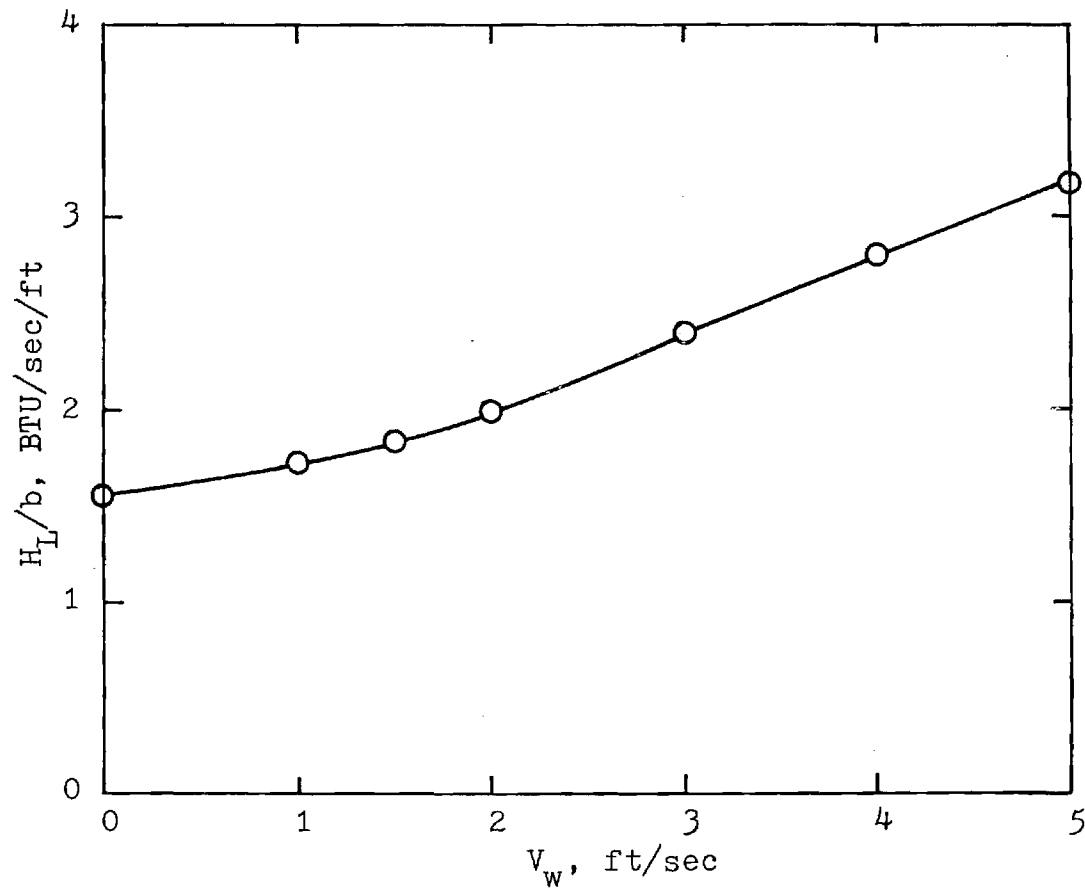
Figure 12. – Example Problem Results for Surface Heat Loss
Rate for Combined Gravity and Wind Driven
Circulations.

3.5 Summary

These results cannot be extended directly to the turbulent case for field cooling lakes because the assumption of a constant eddy viscosity is not a good one for a stratified flow. The results do support the conclusion, however, that gravity currents remain quite important for low speed, intermittent winds which contribute primarily to the processes involved in establishment of stratification in the main body of the cooling lake rather than driving currents. Additional research on the vertical distribution of turbulent eddy viscosity in a stratified flow with applied wind shear is needed to establish a limiting wind speed beyond which only wind-driven currents are important.

4. WIND-INDUCED VERTICAL MIXING

4.1 Introduction

In this chapter the effect of wind in generating turbulent kinetic energy in a stratified cooling lake is considered. A portion of the kinetic energy is utilized in achieving vertical mixing and deepening of the thermocline. Wind stirring will be the primary deepening mechanism considered rather than turbulent entrainment by large wind-driven currents. The stirring mechanism is considered to be of more importance in small, sheltered lakes. A computer simulation model of the vertical stratification in the lake is developed. The model has a daily time step and includes the physical processes of surface heat transfer at the water surface, vertical advection due to cooling water circulation, and wind stirring. Furthermore, a framework for including gravity and wind-driven currents in sidearms is suggested. The model is applied to two small lakes on the University of Notre Dame campus, one of which is used for cooling water while the other is utilized only for recreational purposes. Field data was gathered for these two lakes during the stratification seasons of 1976 and 1978, and the model predictions are compared with the field temperature data.

Previous modeling efforts related to natural thermal stratification of lakes in temperate climates can be divided into two types. The first type of model, exemplified by the work of Orlob and Selna (1970) and Henderson-Sellers (1976), attempts to specify the magnitude and nonuniform distribution of the vertical turbulent thermal diffusivity as related to wind stress, current structure, and thermal stability. The

thermal diffusivity is substituted into the transient, one-dimensional
form of the equation of thermal energy conservation, which is solved
numerically. An alternative approach was suggested by the work of Tur-
ner and Kraus (1967) and was applied by Stefan and Ford (1975) in a lake
stratification model which discretizes the lake into horizontal, isother-
mal layers. In this approach, wind-induced vertical mixing is accounted
for in an integral, energy sense by computing the ratio of kinetic ener-
gy of the wind, which is applied to the lake surface, to the buoyant po-
tential energy of the density stratification. If this ratio exceeds
some critical value, the heat of the upper layers is convectively mixed
downward by entrainment of lower layers into the upper, well-mixed lay-
ers. Octavio, Jirka, and Harleman (1977) added a similar wind-mixing
routine to the M.I.T. Reservoir Model (Ryan and Harleman, 1971), which
formerly did not consider vertical turbulent diffusivity induced by
wind. One of the most comprehensive attempts at modeling the relevant
physical processes of heat transport in a lake is that by Imberger et
al. (1978). This model is a transient, horizontal-slab model which con-
tains a variable time step and a variable layer thickness to account for
the differing time and length scales of important physical mixing pro-
cesses, including wind stirring, wind shear production, penetrative con-
vection, withdrawal, river inflows, and hypolimnetic diffusion.

4.2 Description of the Numerical Model

The numerical model is a horizontal-slab discretization which is
built around four basic physical processes contributing to the heat
balance of a cooling lake: surface heat transfer, wind stirring, ver-

tical advection due to inflows and outflows, and molecular diffusion. The first process to be considered is that of heat transfer at the air-water interface, including absorption of short wave radiation below the free surface. The short wave radiation is distributed exponentially with depth, and the extinction coefficient is determined from measured Secchi disk depths. The empirical relations for determining net solar radiation, atmospheric radiation, back radiation, and conduction as summarized by Ryan and Harleman (1973) are incorporated into the model.

The relation for evaporative heat flux is investigated in some detail. Several equations based on the "mass-transfer approach" are tried in the model. These equations take the general form:

$$\phi_e = \psi(e_s - e_a) \tag{28}$$

in which ϕ_e is evaporative heat flux; e_s is the saturation vapor pressure of air at the temperature of the water surface; e_a is the air vapor pressure at a distance of 2 meters above the water surface, and ψ is a coefficient that may depend upon wind speed and the temperature difference between the water surface and air. Proposed expressions for ψ have been summarized by Paily et al. (1974).

Meteorological data required for the surface heat flux component of the model include daily values of air temperature, dewpoint temperature, wind speed, and degree of cloudiness, which is used with clear sky solar radiation tables for computation of daily incoming solar radiation. The data required are readily available from a National Weather Service Class A weather station in the U.S.

The second major component of the lake thermal model is the vertical

mixing induced by wind. The energy approach suggested by Stefan and
Ford (1975) is utilized in the model. The wind kinetic energy (WKE)
applied to the lake surface is compared to the buoyant potential energy
(BPE) of the lake stratification which must be overcome for vertical
mixing to occur. The mixing criterion is formulated as:

$$WKE \geq r_c \times BPE \qquad (29)$$

for the vertical mixing routine to be initiated, where r_c is some crit-
ical ratio determined by calibration. The wind kinetic energy is com-
puted by:

$$WKE = \tau_s u_* A_s \Delta t = (C_D \rho_a V_{10}^2)^{3/2} A_s \Delta t / \rho_w^{1/2} \qquad (30)$$

in which τ_s is the wind shear stress expressed in terms of a coefficient
of drag, C_D, and the wind speed at a 10-meter height, V_{10}; u_* is the
friction velocity $(\tau_s/\rho_w)^{1/2}$; A_s is the lake surface area; Δt is the
duration of the time period over which working by the wind is considered;
and ρ_a and ρ_w are densities of air and water, respectively. The coeffi-
cient of drag, C_D, is a weak function of wind speed at low speeds and is
affected by atmospheric stability and water depth. Because of the ex-
treme variability in C_D which has been observed in many field studies,
its value is taken to be constant and equal to 1.3×10^{-3} as suggested
by Imberger in Fischer et al. (1979).

The change in buoyant potential energy, which will occur if the
lake is initially completely stratified and then is fully mixed from the
surface down to layer m, is given by:

$$BPE = \sum_{i=1}^{m} \sum_{j=1}^{i} gV_j (i - j + 1) \Delta z (\rho_{i+1} - \bar{\rho}_i) \qquad (31)$$

in which g is gravitational acceleration; V_j is the volume of layer j; Δz is the layer thickness; ρ_{i+1} is the density of the layer just below i layers which are fully mixed; and $\bar{\rho}_i$ is the fully-mixed density of i layers. As illustrated in Figure 13, the inner iteration sums the buoyant potential energy of i fully-mixed layers relative to layer i+1, which is to be entrained. For each daily time step, successive buoyant potential energy changes are summed in the outer summation of Equation (31) as each new layer is entrained into the mixed layer. The outer summation starts with the surface layer as the only mixed layer (m=1) and increments m until the mixing criterion of Equation (29) is satisfied. On days when m mixed layers already exist, the outer summation still begins from m=1 because no contribution to the sum will be made by the upper mixed layers.

The expression in Equation (30) is in reality the work done by the wind stress, all of which may not appear as kinetic energy available for vertical mixing. This is one reason for the need for calibration of the ratio r_c. Stefan and Ford (1975) suggest that r_c should have the value unity but in later work (Ford and Stefan, 1980) it is recognized that r_c may be variable and that it may be necessary to reduce A_s to account for wind sheltering. It has further been suggested by Octavio et al. (1977) that A_s should be represented instead by the surface area at the elevation of the thermocline where the actual wind-induced entrainment occurs. Finally, the measured wind speed, which is required to compute WKE, may be taken from a remote, land-based weather station for which the equilibrium wind velocity profile is different
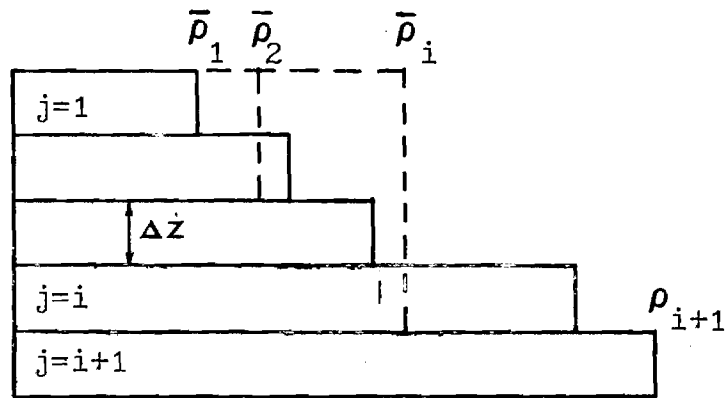
Figure 13. – Definition Sketch for Calculation
of Lake Buoyant Potential Energy
Changes Due to Entrainment

than that for a small lake surface (Hicks, 1975). Because of all these
factors which influence the computation of wind kinetic energy available
for vertical mixing by stirring, the most prudent approach seems to be
to consider r_c a coefficient which must be calibrated for each lake.

The third major component of the simulation model is the vertical
advection which results from inflows and outflows to the lake. The
inflows and outflows for the field cooling lake to which the model is
to be applied are due primarily to the cooling water circulation through
the lake. A portion of the lake inflow is a submerged discharge from
the cooling towers while the remainder is a surface discharge. The
power plant intake is the primary outflow from the lake, and it is
treated as a point of selective withdrawal.

The inflow-outflow subroutine first determines the volume change
in each layer due to inflow and outflow. A heat balance is required
for each layer from which the new layer temperature can be computed.
A mixing routine is then executed in which the layers are adjusted to
their original volumes while maintaining an overall heat balance and
assuming that each layer is individually fully-mixed. The total lake
volume is held constant due to the model application to be described,
but variable lake volume could be accommodated by a simple extension
of the mixing routine.

The outflow from the lake is considered to be a sink which in-
duces a distribution of horizontal velocity that is Gaussian in the
vertical direction and centered on the sink (Huber, Harleman, and Ryan,
1972). The standard deviation of the Gaussian distribution, σ_o, is

computed individually for the density distributions above and below

the sink from the selective withdrawal formula of Elder and Wunderlich

(1969):

$$\sigma_o = 1.28 \left(\frac{\rho_o q_o^2}{g(d\rho/dz)} \right)^{1/2} \tag{32}$$

in which q_o is the outflow per unit width at the level of the intake;

ρ_o is a reference density; and $d\rho/dz$ is the appropriate vertical density

gradient either above or below the intake. From the velocity distribution

so determined, it is then possible to determine the volume withdrawn

from each layer during the daily time step. Some lower limit must be

placed on the value of σ_o to maintain a non-negative layer volume at

the level of the intake, as well as an upper limit defined by the

location of the free surface and bottom of the lake.

Submerged inflow to the lake is treated as a submerged buoyant

jet with entrainment. An entrainment coefficient is specified for

each layer, and the entrainment withdrawal from each layer is thus

known. A heat balance is computed for the jet until its temperature

and hence density is equal to the surrounding ambient density. At

this point the total jet flow, including the entrained flow, is

distributed by a vertical Gaussian distribution with σ_I specified

according to the geometric jet characteristics. The entrainment

jet algorithm is applicable for either a positively or negatively

buoyant jet.

A small surface inflow occurs through a diffuser submerged just

below the water surface and located in a shallow discharge channel

(3 ft. deep) in the lake to be studied. The field temperature measurements, to be described subsequently, indicated nearly complete vertical mixing in the discharge channel and agreed well with a plug-flow model. At the outlet of the discharge channel into the lake, the Froude number was not sufficiently large to indicate any substantial surface jet entrainment. At this point, the computer simulation model takes the predicted temperature output from the plug-flow computation and uses a Gaussian velocity distribution to generate inputs for the inflow-outflow subroutine described previously.

The fourth and final component of the simulation model is vertical mixing due to molecular diffusion. This portion of the model determines the daily vertical heat transfer between layers due to molecular diffusion and adjusts the layer temperatures accordingly. The addition of molecular diffusion was found to smooth the model temperature profiles and to have some influence on the bottom temperatures attained by late summer and early fall.

These four components of the lake heat balance are combined into a sequential algorithm that is repeated on a daily basis as shown in Figure 14. Stefan and Ford (1975) found that the order in which the surface heat flux and wind-mixing routines are executed does not in general affect the results for the daily mean thermal structure of the lake. This was also found to be true for the inflow-outflow routine added to the present model. If model results are compared to a single daily measurement of temperature profiles, on the other hand, some

```
┌─────────────────────────────────┐
│ READ DAILY METEOROLOGICAL       │
│                                 │
│ AND LAKE INFLOW DATA            │
└─────────────────────────────────┘
                 │
                 ▼
┌─────────────────────────────────┐
│ COMPUTE LAYER TEMPERATURE       │
│                                 │
│ CHANGES DUE TO SURFACE HEAT     │
│                                 │
│ FLUX AND RADIATION ABSORPTION   │
└─────────────────────────────────┘
                 │
                 ▼
┌─────────────────────────────────┐
│ DETERMINE TEMPERATURE CHANGES   │
│                                 │
│ DUE TO INFLOWS AND OUTFLOWS     │
└─────────────────────────────────┘
                 │
                 ▼
┌─────────────────────────────────┐
│ APPLY WIND MIXING ROUTINE       │
└─────────────────────────────────┘
                 │
                 ▼
┌─────────────────────────────────┐
│ RELAX TEMPERATURE PROFILE       │
│                                 │
│ BY MOLECULAR DIFFUSION          │
└─────────────────────────────────┘
                 │
                 ▼
          ┌───────────┐
          │ WRITE     │
          └───────────┘
                 │
                 ▼
  no      ┌───────────────┐
 ─────────│ END OF DATA?  │
          └───────────────┘
                 │ yes
                 ▼
            ┌────────┐
            │ STOP   │
            └────────┘
```
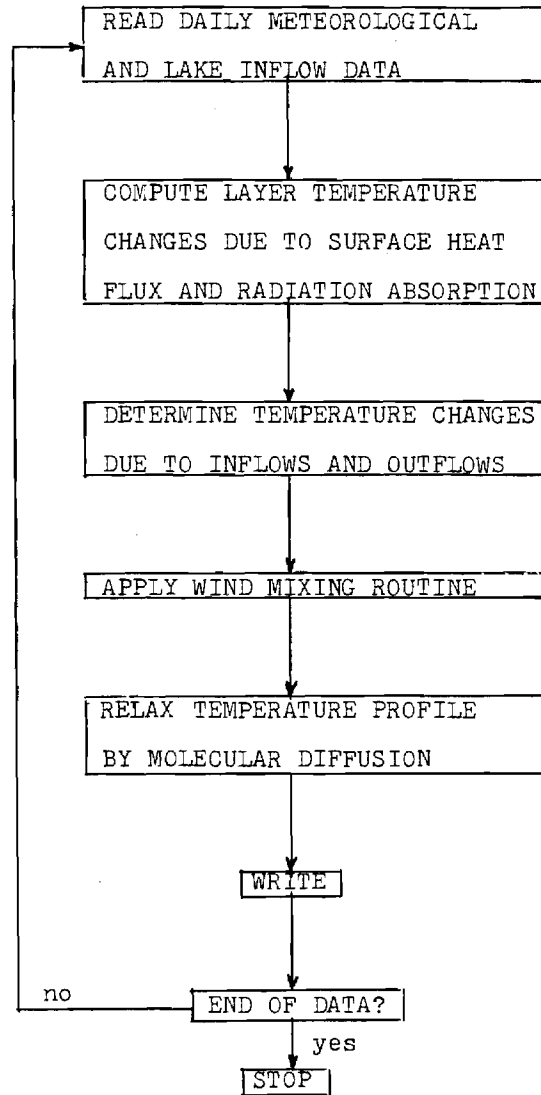
Figure 14. – Flow Chart for Lake Simulation
Model.

discrepancies may result between measured data and model results

because of the hourly variation in wind speed and surface heat flux.

In spite of these discrepancies, a model of daily mean thermal

structure is often sufficient to make lake management decisions, and

so the additional difficulty of obtaining and using hourly meteor-

ological data was not considered to be warranted for the purposes

of this study.

4.3 Field Investigation

Temperature data were obtained in 1976 and 1978 for two small

lakes located adjacent to each other on the University of Notre Dame

campus. St. Joseph's Lake is used for swimming, sailing, and as a

cooling water source for the University power plant, which provides

both electric power and chiller air conditioning in the summer for

campus buildings. As shown in Figure 15, the cooling water intake is

approximately 25 ft deep and cooling water is discharged both

through mechanical draft cooling towers and a surface discharge

structure. A fixed discharge of 12,000 gpm is directed through the

cooling towers and back into the lake through a 4-ft diameter pipe

located approximately 8 ft deep in the east end of the lake. Any

excess cooling water flow, which varies from 1000 to 2000 gpm, is

diverted to the surface discharge diffuser located in shallow water

near one of the islands at the west end of the lake. This mode

of operation is followed throughout the air-conditioning season.

In winter, early spring, and late fall, however, cooling water is
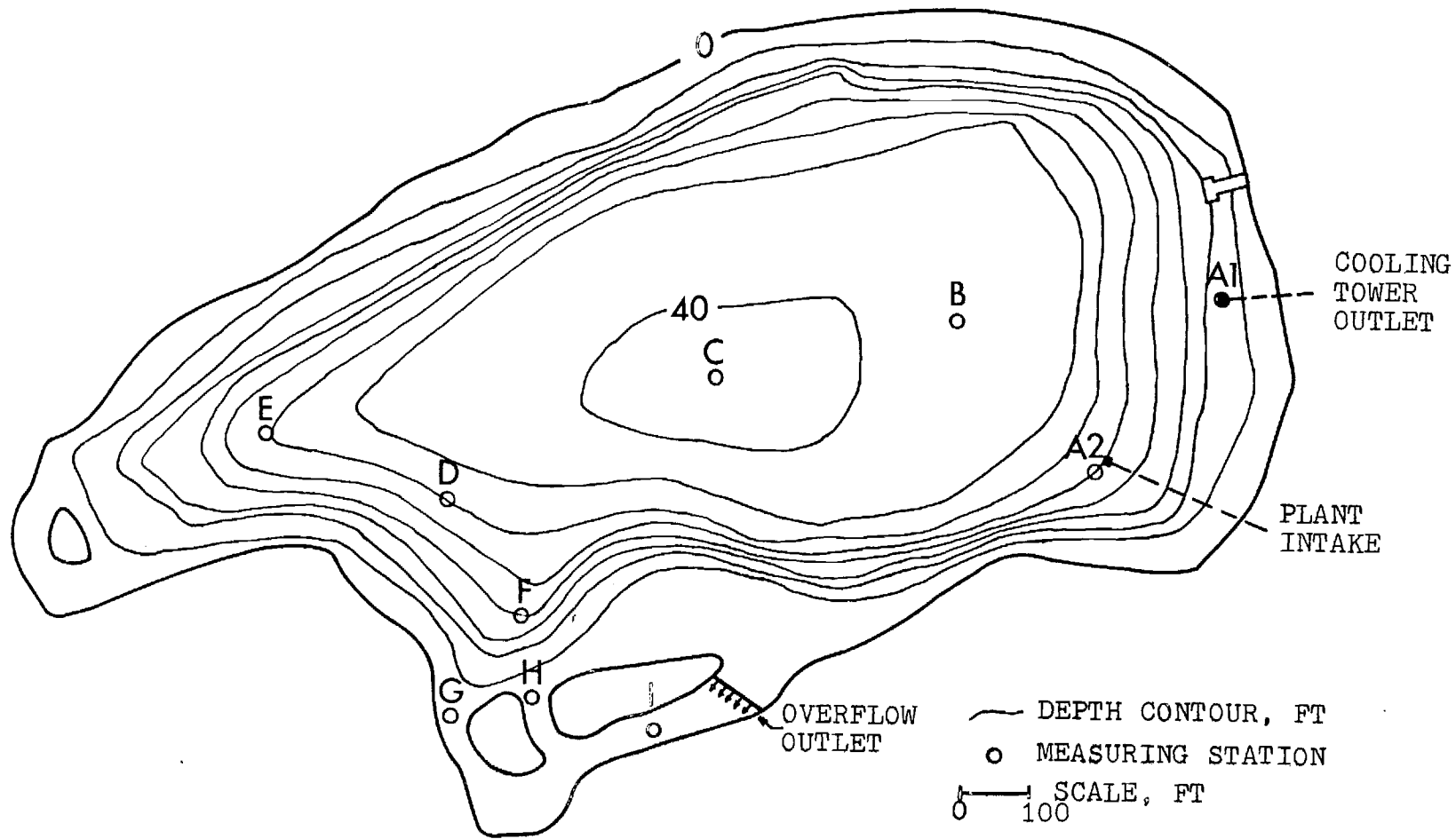
Figure 15. — St. Joseph's Lake Depth Contours and Measuring Stations

needed only for condensation of spent steam used in power generation.
During these time periods, the cooling towers are not operated and
the entire condensor discharge goes to the surface-discharge structure.

St. Joseph's Lake has a surface area of 26 acres and is located
adjacent to St. Mary's Lake, which has a surface area of 21 acres.
Both lakes are spring-fed and receive very little surface runoff.
Their water surface levels are nearly constant throughout the year.
The cooling water discharge in winter is sufficient to maintain a
small ice-free area near the islands in St. Joseph's Lake except in
the most severe winters.

Vertical temperature profiles were measured from a boat at the
locations shown in Figure 15 for St. Joseph's Lake from spring through
early fall in 1978 and throughout the summer and fall of 1976.
Measuring locations were identified by bottom-anchored, surface buoys.
Temperatures were also measured at a single location in St. Mary's
Lake during August, 1976. A battery-powered temperature indicator
and a thermistor probe were used to measure the water temperatures
with an accuracy of $\pm 0.5°C$ at 5-ft vertical intervals at each
measuring location. Daily meteorological data were obtained from
a Class A weather station located at the South Bend, Indiana airport
approximately five miles west of the lakes.

Measured temperature rises through the chiller and generator
cooling systems are shown in Figure 16. These data were obtained
from hourly power plant records. The computed discharges through
the generator and chiller cooling systems are shown in Figure 17.

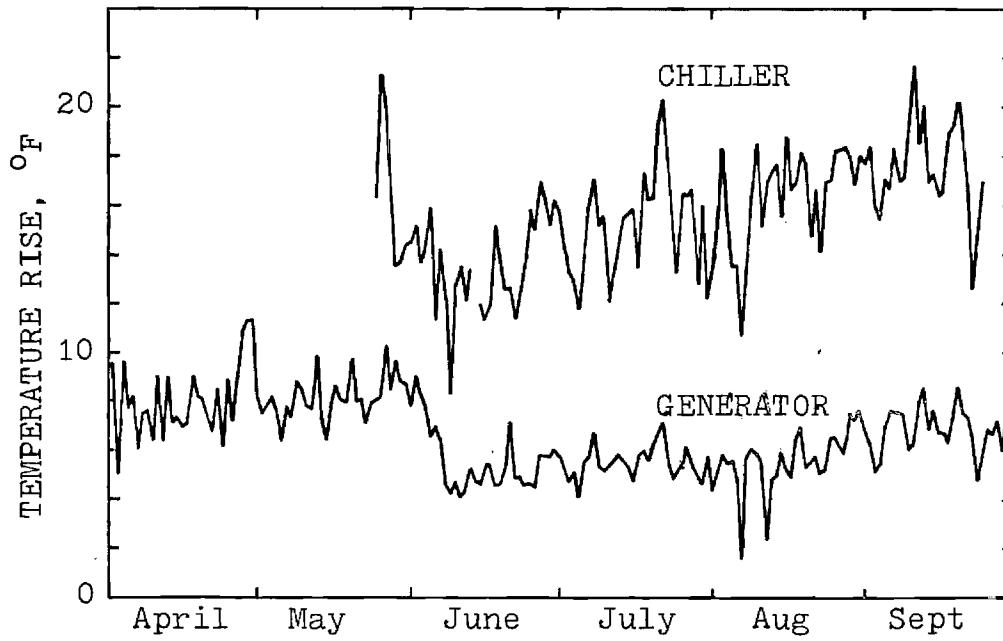Figure 16. - Power Plant Condensor Temperature Rises, 1978.
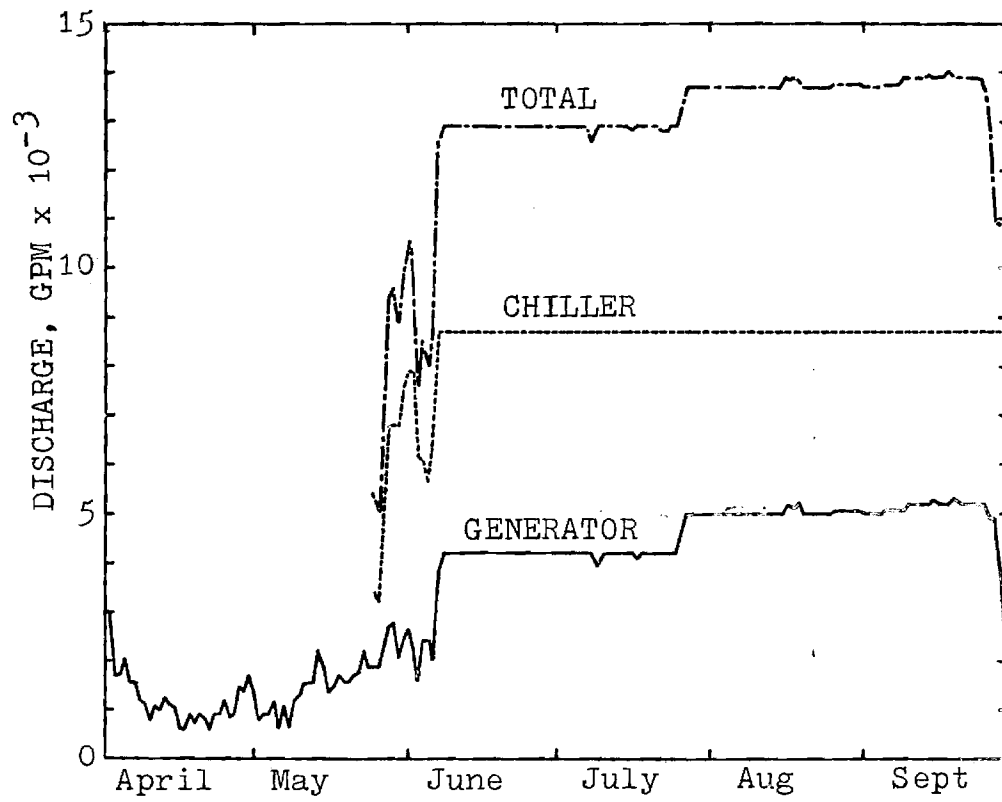
Figure 17. - Power Plant Condensor Discharges, 1978.

Power plant records included data on butterfly control valve positions.

These valve positions were calibrated by measuring the corresponding

discharges through the overflow discharge pipe with a current meter.

The discharges and their temperatures from the generator and chiller

condensors were combined to produce daily values of fully-mixed

discharges of known temperature in the simulation model. When the

cooling towers were in operation, the simulation model diverted

12,000 gpm through them with an assumed constant cooling range of

12°F and allocated the remainder to the surface discharge structure.

Measured input and output temperatures for the cooling tower during

August, 1976 indicated an average cooling range of 12°F ± 2°F,

and so it was assumed constant in the model. Although it would be

possible to model the cooling range on a daily basis as described by

Croley et al. (1976), the available input data was considered in-

sufficient to warrant this detailed approach. If a lake simulation

model such as that described herein were to be used in the detailed

planning and design stages of cooling tower additions to a cooling

lake, then detailed thermodynamic modeling should be included.

The applicability of a horizontal slab model as proposed herein

depends upon whether or not the isotherms can be considered essentially

horizontal throughout the stratification period. Isotherms determined

from measured temperatures are shown in Figures 18 and 19 for the

months of June and August 1976 in St. Joseph's Lake. Although a

small region of heat input is apparent near the islands, the isotherms

are approximately horizontal. Most of the artificial heat input is being
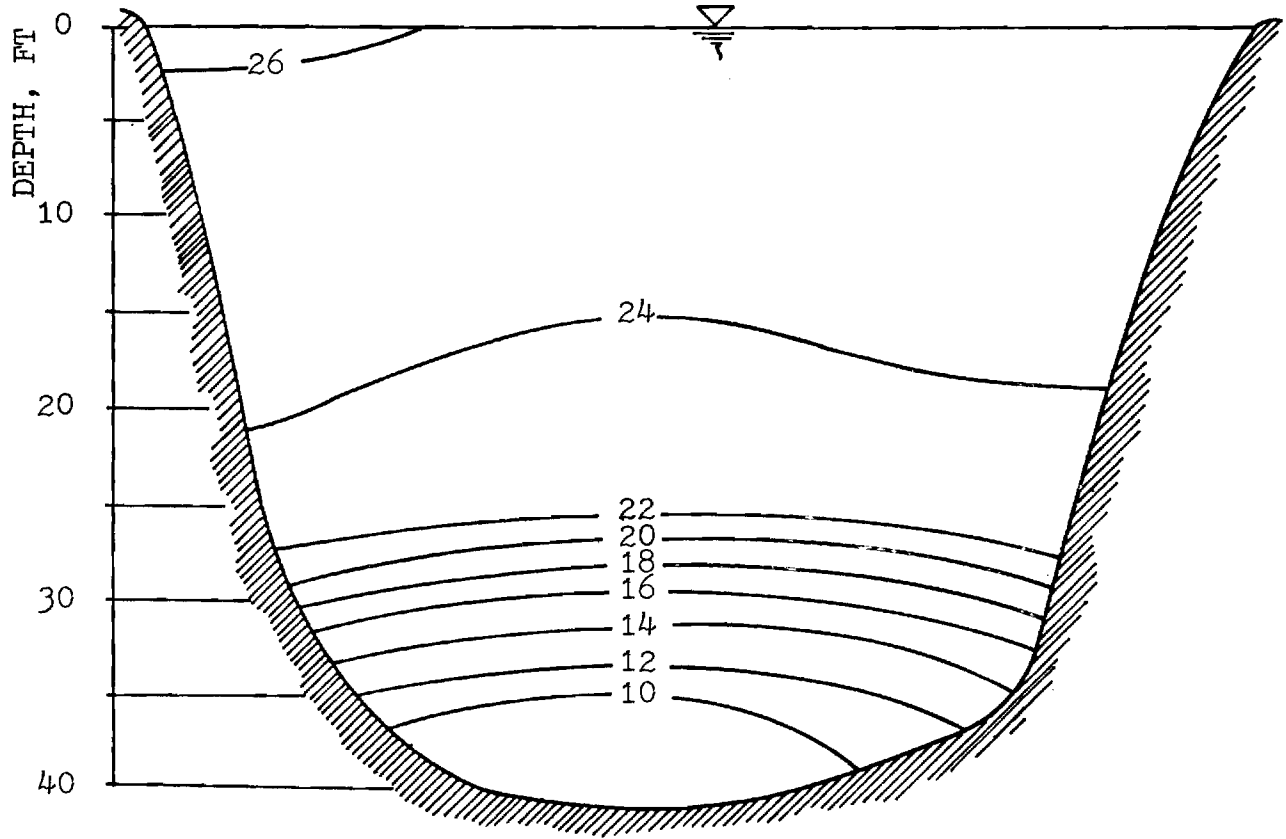
Figure 18. – Measured Isotherms, °C, in St. Joseph's Lake, June, 1976.
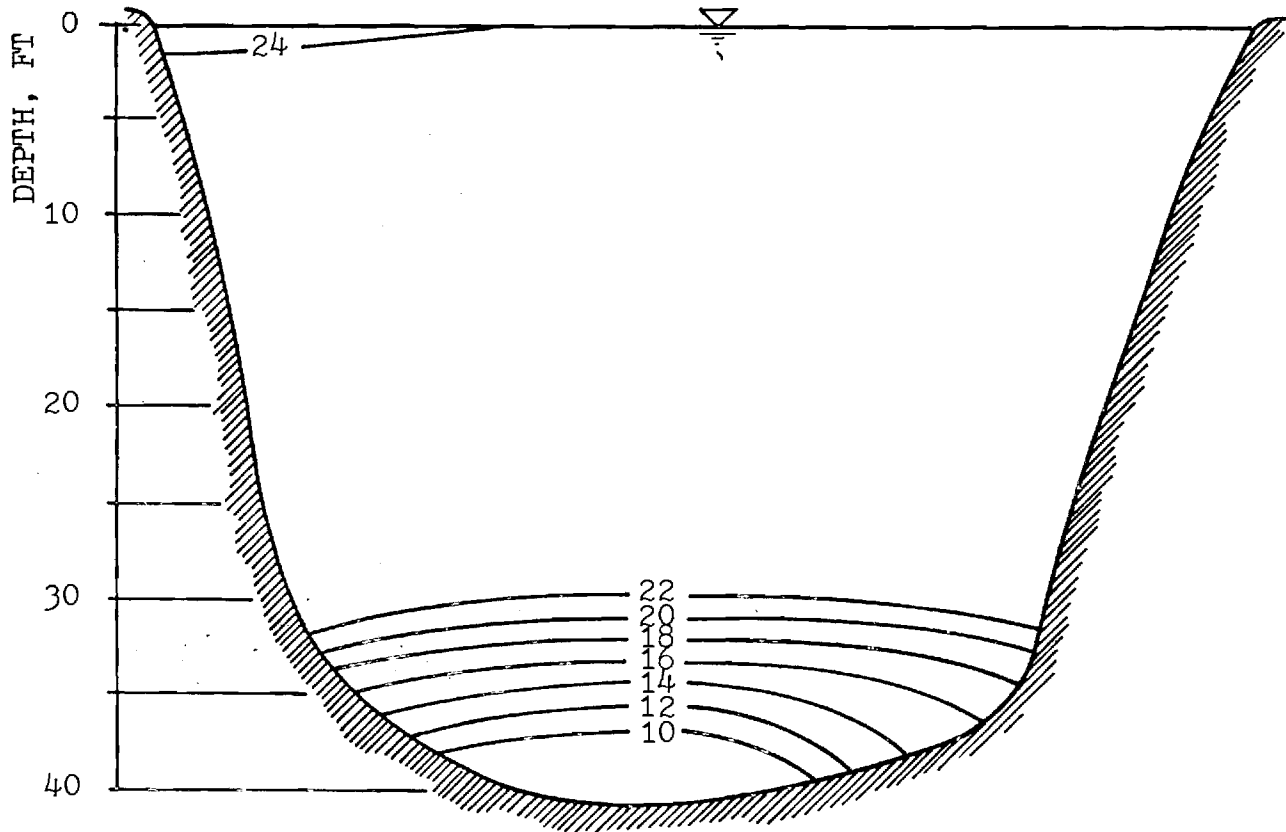
Figure 19. - Measured Isotherms, °C, in St. Joseph's Lake, August, 1976.

dissipated to the atmosphere near the islands and horizontally

mixed by the cooling tower operation. In a conventional cooling

lake without "helper" cooling towers, the assumption of horizontal

isotherms cannot be made for a surface, heated discharge into the

epilimnion.

One of the major components of the model as described herein

is the wind-mixing routine, which considers the wind to be a surface

stirring agent that provides kinetic energy for vertical mixing.

The effects of shear production at the thermocline by strong winds,

as discussed by Imberger in Fischer et al. (1979), are not considered.

A classification of St. Joseph's Lake according to the scheme

proposed by Spigel (1978) confirms that this assumption is appropriate.

The lake falls into Spigel's regime A which is characterized by very

slow, turbulent erosion of the thermocline with a nearly horizontal

interface.

4.4 Numerical Model Calibration

As discussed previously, the several factors which affect the

computation of wind kinetic energy require calibration of the model,

or in other words, determination of r_c in Equation (29). This

cannot be accomplished in St. Joseph's Lake alone because the

effect of artificial heat input and vertical circulation due to

power plant operation cannot be separated from wind effects to

determine r_c. The existence of a rather unique situation, in which

the adjacent St. Mary's Lake is nearly the same size and has

approximately the same physical orientation to the prevailing wind,

enabled the determination of r_c in St. Mary's Lake due to wind

effects alone. This value was then assumed to apply in St. Joseph's

Lake as well.

The simulation model was executed with daily meteorological

data for 1976 and an initial isothermal condition on April 1,

1976 with only surface heat transfer, wind-mixing, and molecular

diffusion routines included. The predicted temperature profiles

are compared with three measured profiles in St. Mary's Lake for

August, 1976 in Figure 20. The value of r_c required to obtain the

fit shown in Figure 20 is 0.58 with $C_D = 1.3 \times 10^{-3}$ in Equation (30),

and with no adjustment made to the wind speed or lake surface area.

The extinction coefficient has a value of 0.5 ft^{-1} based on the

Secchi disk depth.

The results shown in Figure 20 are for two different evaporative

heat flux relations:

$$\psi_{PL} = 16.2 \; V_2 \qquad\qquad (33)$$

$$\psi_Z = 43. + 14 \; V_2 \qquad\qquad (34)$$

in which ψ_{PL} is the Pretty Lake coefficient (Ficke, 1972); ψ_z

is the Zaykov coefficient (Paily, 1974); V_2 is the windspeed in mph

at a 2-m height; and ψ is the coefficient defined in Equation (28)

with units of $BTU/(ft^2 - day - mmHg)$. The Zaykov formula includes

a free-convection component and tends to overestimate the surface heat

loss with a resultant lower surface temperature. Better agreement between
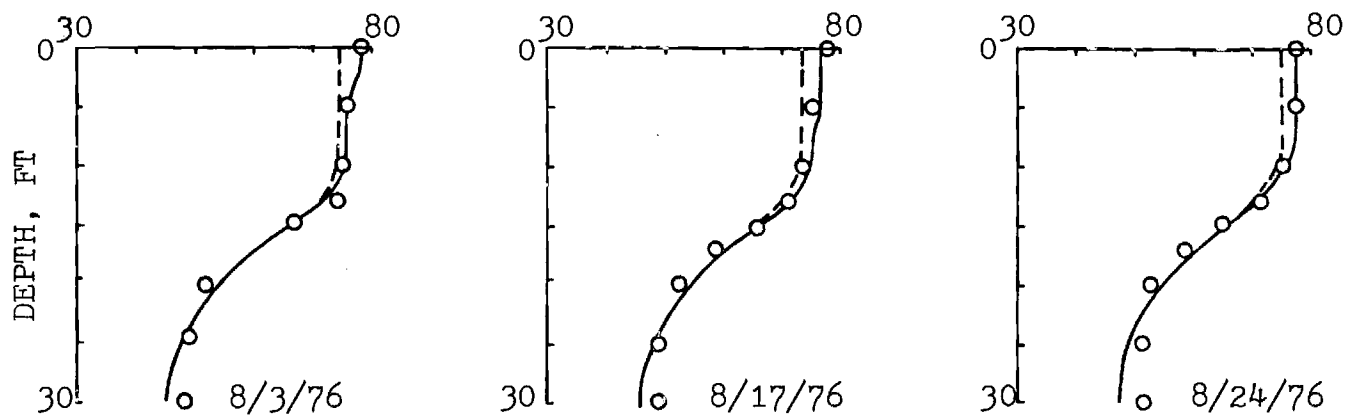
Figure 20. - Comparison Between Measured and Simulated Temperatures in St. Mary's Lake, r_c = 0.58 (O = Measured Temperature;—Model Results, $\psi=\psi_{PL}$; ---Model Results, $\psi=\psi_z$).

measured and predicted surface temperatures is obtained with the
Pretty Lake formula, which was developed from a detailed energy
budget of Pretty Lake, a small natural lake in northeastern
Indiana.

Predicted temperature profiles for different values of r_c
are compared with St. Mary's Lake data in Figure 21. In each case,
the simulation model was started from an isothermal condition in
the spring. The temperature profiles are sufficiently sensitive to
r_c to indicate that it is a useful parameter for characterizing
wind mixing.

The value of r_c of 0.58 is slightly more than half the value
predicted by the laboratory experiments of Kato and Phillips (1969)
in which surface shear was produced by a rotating plate at the
surface of a fluid in an annular container. The experiments of
Wu (1973), in which a wind shear was developed at the water surface
in a very small laboratory flume, predict a value of r_c which is an
order of magnitude smaller than the value based on the experiments of
Kato and Phillips. Wu's coefficient is recommended by Imberger et
al. (1978), but it seems doubtful that a single value of r_c can be
applied to all lakes. All of the factors involved in estimating the
production of kinetic energy by wind stress applied to a lake surface
are bound to show some variation and result in a variable value of
r_c. These factors include wind fetch, wind sheltering, and differences
between water surface and land roughness in the case of a land-based
meteorological station. Ford and Stefan (1980) have suggested a
correction to wind speed to account for fetch and surface roughness

TEMPERATURE, °F

DEPTH, FT

8/3/76   8/17/76   8/24/76
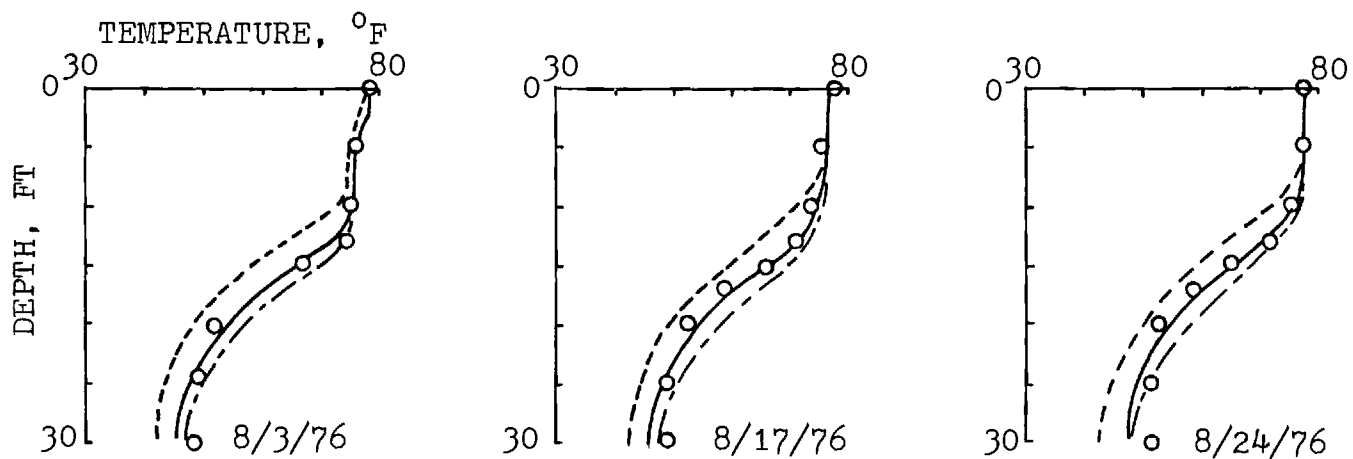
Figure 21. – Comparison Between Measured and Simulated Temperatures in St. Mary's
Lake for Variable r_c.

o Measured Temperature
——— r_c = 0.58
– – – r_c = 1.0
— – – r_c = 0.50

effects, but wind sheltering effects, which are especially important for small lakes, can only be determined by calibration. The unique opportunity offered by the field study of St. Mary's Lake is its similarity to St. Joseph's Lake with respect to the factors which cause r_c to be variable.

4.5 Results for St. Joseph's Lake

Because of the relatively small horizontal temperature gradients existing in St. Joseph's Lake as discussed previously, the simulation model results were compared with measured temperatures at station C at the deepest portion of the lake (see Figure 15). These temperatures were considered to be reasonably representative of the mean vertical thermal structure of the lake. THe simulation model was started from the isothermal condition in spring as for St. Mary's Lake. The value of r_c determined from the wind-mixing calibration fo St. Mary's Lake was also used for the St. Joseph's Lake thermal simulations. The model was similar to the St. Mary's Lake model in all respects except for the addition of the inflow-outflow subroutine which included both surface and submerged cooling water discharges. The complete set of temperature data gathered in 1976 and 1978 for St. Jospeh's Lake is summarized in Table 3 in the appendix.

The simulation model results are compared with the measured 1978 temperature profiles at station C in Figure 22. The Zaykov formula for ψ to determine evaporative heat flux, Equation (34), was used in the computation of the simulation results which are shown in
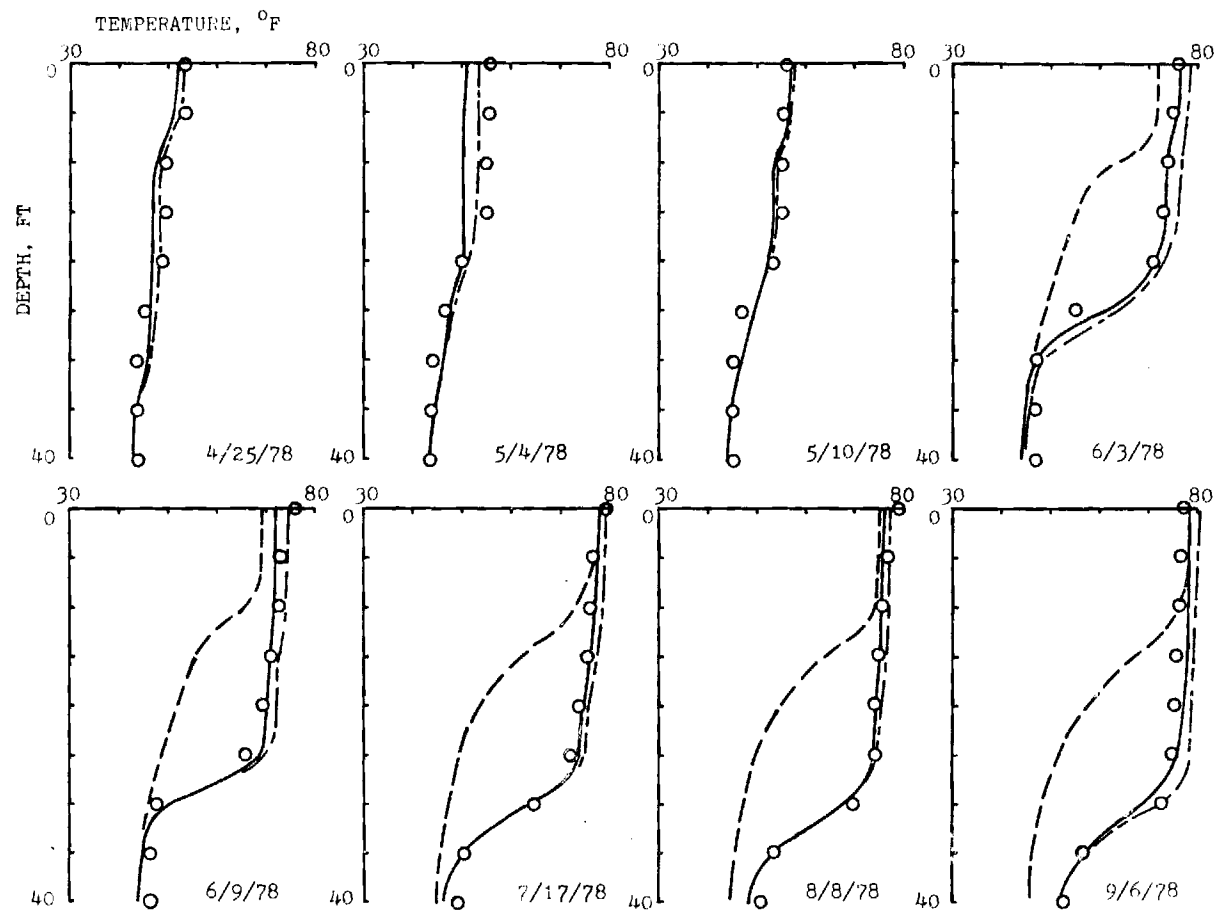
Figure 22. - Comparison Between Measured and Simulated Temperatures
at Station C, St. Joseph's Lake, r_c = 0.58.

o   Measured Temperature ———— - ———— $\psi=\psi_{PL}$

———— $\psi=\psi_z$ — — — — — — Simulated Natural Temperature

Figure 22 by solid curves. These results were essentially unchanged

by using the expression for ψ proposed by Ryan and Harleman (1973)

for cooling ponds. The predicted temperatures agree quite well with

the measured data. The dashed curves in Figure 22 indicate simulation

results without the inflow-outflow subroutine. The Pretty Lake

formula, Equation (33), is used in this case to simulate natural

lake temperatures.

Too much wind mixing by the model is apparent on May 4, but

the general development of stratification from April until mid-

May is modeled well. Beginning on June 3, a considerable dis-

crepancy develops between the modeled natural lake temperatures

and the actual temperatures resulting from cooling operations. The

reason for this discrepancy becomes apparent by referring to Figure

17, which indicates a significant rise in power plant discharges to

the lake in late May. This results in substantial mixing by

vertical advection and accounts for the deepening of the thermocline

on June 9, and the simulation results indicate that the model

adequately accounts for this effect by addition of the inflow-out-

flow routine. From mid-July until early September the measured

data and simulation results show a fairly stable temperature profile.

During this time period, the power plant discharges shown in Figure

17 are relatively constant. The simulation results indicate that

power plant cooling operations have increased the epilimnion thick-

ness from a natural value of 10 to 15 ft to a much larger value of

nearly 30 ft. The simulation model results were found to be

relatively insensitive to the jet entrainment coefficients for the

cooling tower discharge, especially in the case of a positively
buoyant jet which essentially acted as an aid to full vertical
mixing of the upper portion of the epilimnion.

Simualtion model results for 1978 are also shown in Figure 22
with evaporative heat flux determined by the Pretty Lake formula.
Although it improves surface temperature predictions in spring when
power plant operations are minimal, it overestimates the epilimnion
temperatures in late summer and early fall. The Pretty Lake
formula contains no free-convection component and thus underestimates
the surface heat loss for low wind speeds.

Simulation results are compared with measured temperature data
for 1976 in Figure 23. The simulation model includes the inflow-
outflow routine, and 1976 power plant data and meteorological data
are used as inputs. The model is started from an isothermal
condition in early spring as for the 1978 data. The agreement
between predicted and measured temperature profiles is again quite
satisfactory.

A dimensional analysis for the depth to the thermocline is
instructive in emphasizing the relative influence of wind mixing
and vertical advection in St. Joseph's Lake. If h is defined as
the depth to the thermocline, we have:

$$h = f(D, L, B, u_*, g', Q_o) \tag{35}$$

where D = lake depth; L = lake length; B = the average width of the
lake at the outlet; u_* = friction velocity due to wind currents;
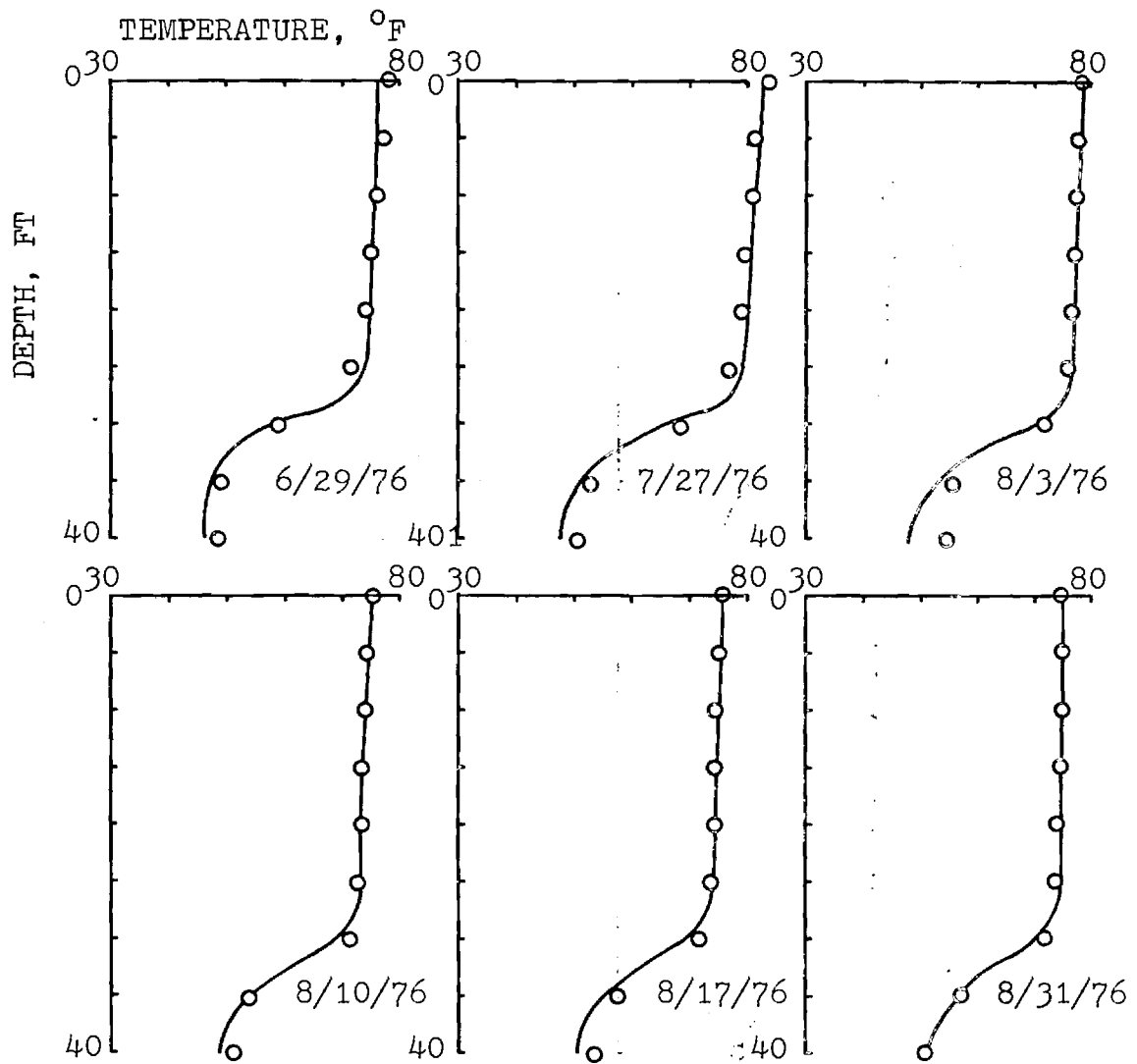
Figure 23. — Comparison Between Measured and Simulated
Temperatures at Station C, St Joseph's Lake,
1976, r_c = 0.58.

$g' = (\Delta\rho/\rho)g$; $\Delta\rho$ = the density difference between the water surface and the hypolimnion; and Q_o = the lake withdrawal discharge. Dimensional analysis produces:

$$\frac{h}{D} = f_1\left(\frac{L}{D}, \frac{B}{D}, \frac{g'D}{u_*^2}, \frac{Q_o^2}{g'B^2D^3}\right) \tag{36}$$

in which $g'D/u_*^2$ represents a wind current Richardson number, Ri_*; and $Q_o^2/g'B^2D^3$ is a withdrawal densimetric Froude number, F_D. For a given lake, L/D and B/D are relatively constant, and only the Richardson number and densimetric Froude number indicate the influence of wind, surface heating, and withdrawal on the development of stratification. The variable $\Delta\rho$ appears as an independent variable in (36) but it is really determined by the surface heat transfer processes and so it reflects their effects, relative to wind and inflow-outflow effects.

The values of $Ri_*^{-1/2}$ and F_D were determined on a daily basis from the computer simulation model and are shown in Figures 24 and 25. Decreasing values of these parameters indicates increasing stability relative to vertical mixing. In early summer, there is a very apparent increase in F_D due to cooling tower operation and a marked decrease in $Ri_*^{-1/2}$. This indicates a greater stability with respect to wind but decreased stability due to power plant cooling water circulation. The response of the thermal lake structure is a relatively abrupt deepening of the epilimnion as shown in Figure 22.
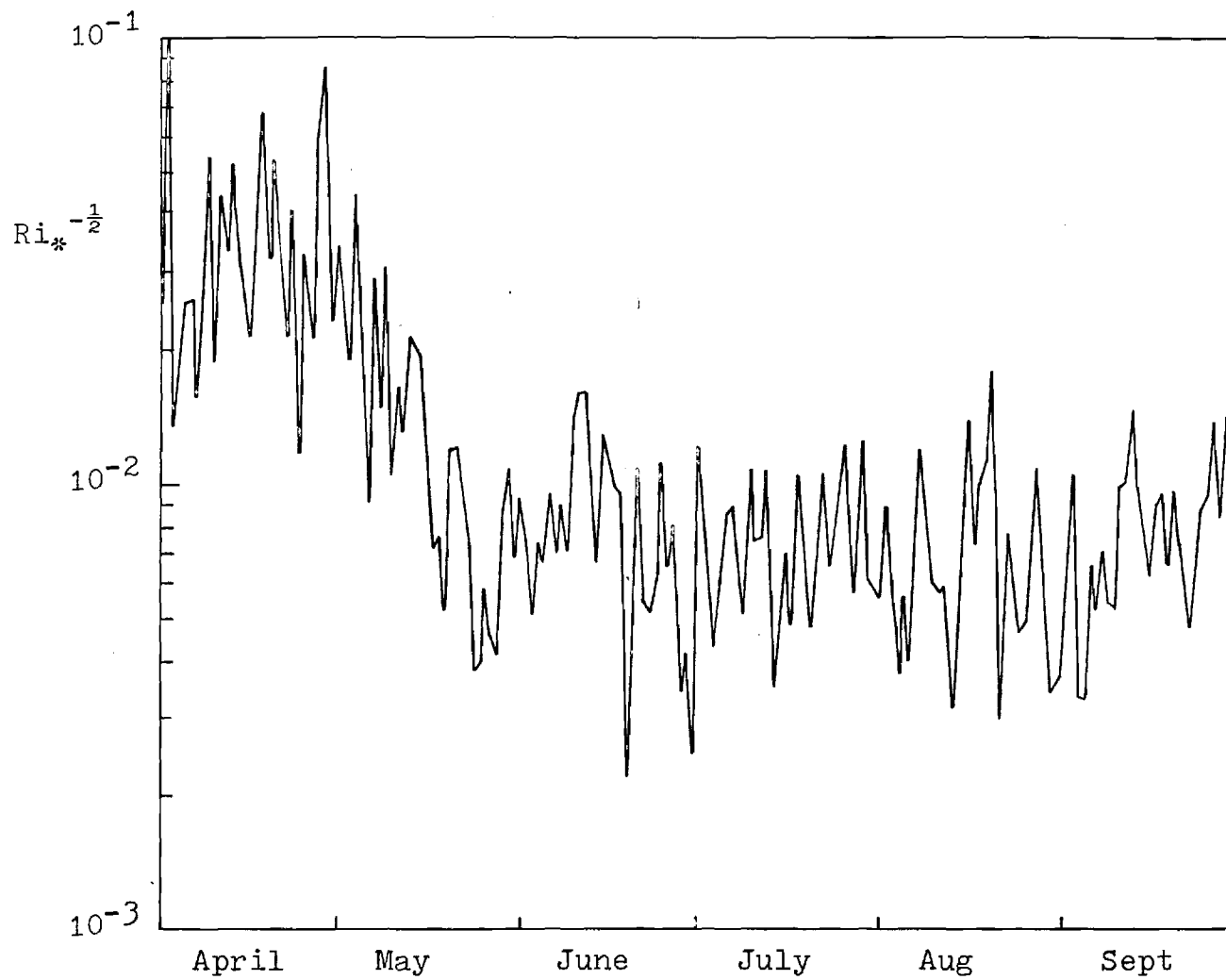
Figure 24. – Model Results for Wind
Richardson Number, Ri_*, 1978.
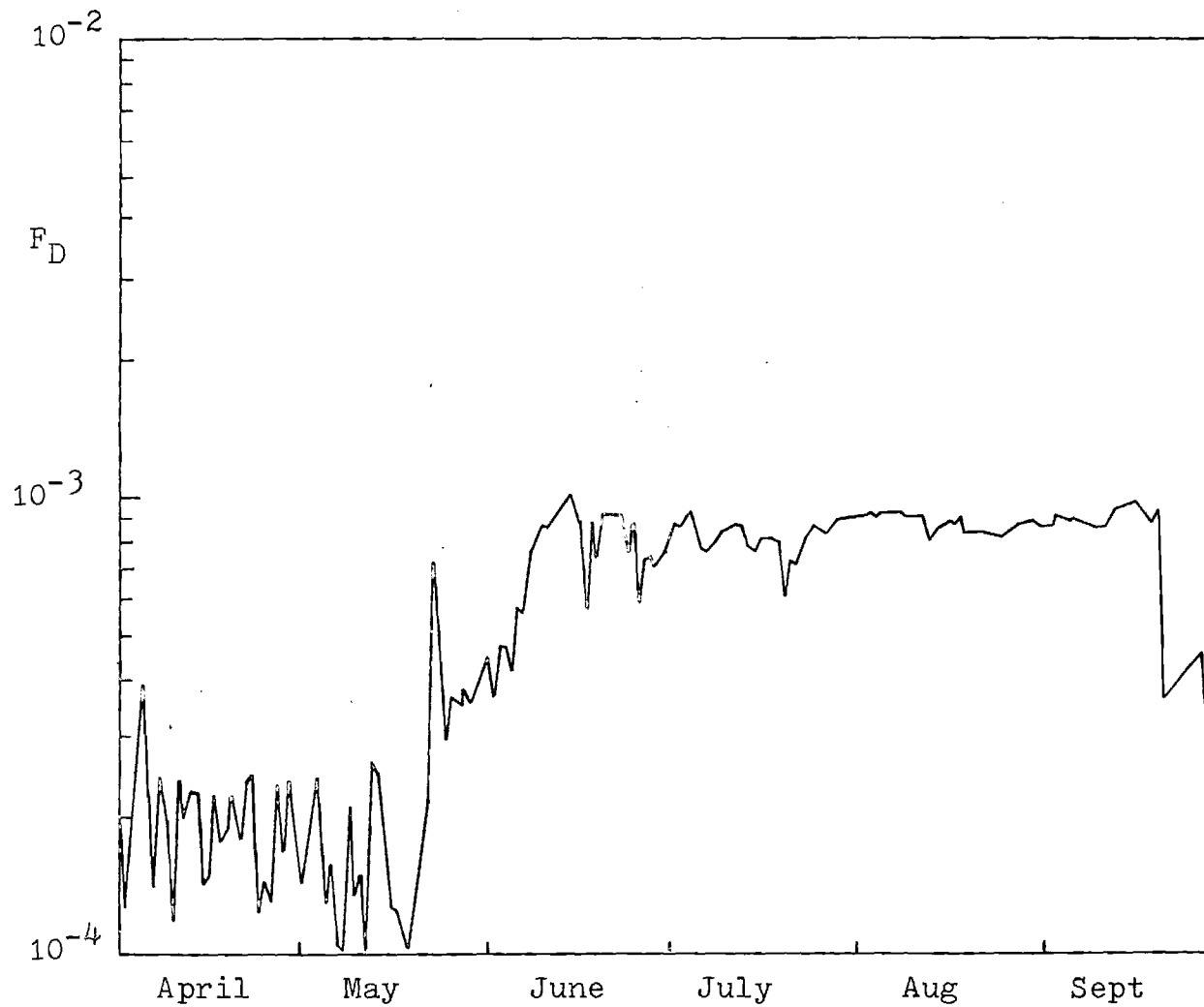
Figure 25. – Model Results for Outflow Densimetric
Froude Number, F_D, 1978.

4.6 Combining Gravity Current and Lake Stratification Models

The structure of the computer simulation model developed herein is such that the effects of gravity and wind-driven currents can be easily added in the surface heat loss subroutine to account for sidearm heat losses. The analysis in Chapter 3 suggests that a limiting windspeed can be determined beyond which only wind-driven current effects need be considered in the sidearm. For smaller wind-speeds, a model similar to that developed in chapter 3 is needed with the consideration of turbulent flow rather than laminar flow. Because much additional research is necessary to define the vertical distribution of eddy viscosity due to combined wind shear and bottom production of turbulence, and further because sidearm effects were not important in the field lake studied, these effects have not been incorporated into the simulation model application described in this chapter.

4.7 Summary

A simulation model of the vertical thermal stratification of a cooling lake has been developed in this chapter. The model includes the effects of surface heat transfer, wind mixing, vertical advection due to inflows and outflows, and molecular diffusion. When applied to a field cooling lake after having been calibrated on a natural lake, the model clearly indicates the dominant effect of cooling water circulations on establishment of the epilimnion thickness. The epilimnion is shown to be significantly thicker due to cooling water circulations. This occurs despite the fact that the cooling

towers adequately dissipate most of the excess heat before discharging
to the lake. The relative influence of wind mixing and vertical
advection on lake stability for a particular lake is illustrated
by the introduction of two dimensionless numbers: a wind Richardson
number and an outflow densimetric Froude number. Finally, it is
suggested that a turbulent model of combined wind and gravity
currents be added to the simulation model discussed in this chapter
to determine sidearm heat losses when appropriate.

5. SUMMARY AND CONCLUSIONS

A closed-form solution for laminar gravity currents in dead-end channels has been presented and verified with laboratory data. In practice, these currents are the result of thermally-induced buoyancy and would be expected to occur in cooling lake sidearms. The closed-form solution provides an estimate of the total rate of surface heat loss from the sidearm gravitational circulation. Using the same problem formulation, a surface wind stress directed toward the dead end of the sidearm has been added as a boundary condition at the free surface. A numerical solution of the resulting equations clearly shows the interaction between wind-driven and buoyancy-driven circulations. Relations for surface heat loss for a combined circulation are developed from the numerical results. By means of an example, it is shown that as wind speed is increased, a limiting wind speed is reached beyond which the wind-driven current becomes dominant and the surface heat loss rate in the sidearm is the same as in the cooling lake at the sidearm entrance.

The effect of wind stirring on the development of vertical stratification in a cooling lake is also investigated. A computer simulation model is developed using an energy approach to vertical mixing by wind. The model also includes vertical advection of heat due to inflows and outflows from the lake. The model is applied to a natural lake and to an adjacent cooling lake, for which field data were obtained, and it is concluded that vertical advection is primarily responsible for the observed thermal structure of the cooling lake. A dimensionless Richardson number and Froude number are proposed to show the relative influence of wind mixing and vertical advection.

Inclusion of gravity and wind-driven currents was not necessary to predict the observed mean thermal behavior of the field cooling lake studied; however, in other cases in which significant sidearm area occurs and artificial heat inputs are large, it is concluded that these currents are quite important to the overall surface heat loss rate. The present structure of the thermal lake simulation model, and the presentation of the results for surface heat loss rates for combined wind-driven and gravitational circulations in sidearms, would allow incorporation of these heat loss rates into the simulation model. Additional research is needed, however, on the vertical distribution of turbulent eddy viscosity in a stratified flow with both wind and bottom-generated turbulence before this step is taken.

REFERENCES

1. Baines, W.D. and Knapp, D.J., "Wind Driven Water Currents,"
   J. Hydraulics Div., ASCE, Vol. 91, No. HY2, March, 1965, pp.
   205-221.

2. Banks, R.B., "Some Features of Wind Action on Shallow Lakes,"
   J. Env. Engineering Div., ASCE, Vol. 101, No. EE5, October, 1975,
   pp. 813-827.

3. Benjamin, T.B., "Gravity Currents and Related Phenomena," J. Fluid
   Mech., Vol. 31, 1968, pp. 209-248.

4. Brocard, D., Jirka, G.H., and Harleman, D.R.F., "Buoyancy-Driven
   Circulations in Side-Arms of Cooling Lakes," presented at the
   Nov., 1975, ASCE Annual Convention, Denver, Colorado.

5. Brocard, D.N., Jirka, G.H., and Harleman, D.R.F., "A Model for the
   Convective Circulation in Side-Arms of Cooling Lakes," Report No. 223,
   R.M. Parsons Laboratory, M.I.T., Cambridge, Mass., March, 1977.

6. Cormack, D.E., Leal, L.G., and Imberger, J., "Natural Convection in
   a Shallow Cavity with Differentially Heated End Walls, Part I.
   Asymptotic Theory," J. Fluid Mech., Vol. 65, 1974, pp. 209-229.

7. Croley, T.E., Patel, V.C., and Cheng, M.S., "Thermodynamic Models
   of Dry-Wet Cooling Towers," J. Power Div., ASCE, Vol. 102, No. PO1,
   January, 1976, pp. 1-19.

8. Elder, R.A. and Wunderlich, W.O., "The Prediction of Withdrawal Layer
   Thickness in Density Stratified Reservoirs," Proc. 13th Congress,
   IAHR, Kyoto, Japan, Vol. 2, Sept., 1969, pp. 309-316.

9. Ficke, J.F., "Comparison of Evaporation Computation Methods, Pretty
   Lake, Lagrange County, Northeastern Indiana," USGS Prof. Paper
   686-A, 1972.

10. Fischer, H.B., List, E.J., Koh, R.C.Y., Imberger, J., Brooks, N.H.,
    Mixing in Inland and Coastal Waters, Academic Press, N.Y., 1979

11. Ford, D.E., and Stefan, H.G., "Thermal Predictions Using Integral
    Energy Model," J. Hydraulics Div., ASCE, Vol. 106, No. HY1, January,
    1980, pp. 39-55.

12. Giaquinta, A.R., Croley, T.E., and Hsu, T.D., "Hybrid Cooling System
    Thermodynamics and Economics," J. Energy Div., ASCE, Vol. 106,
    No. EY1, April, 1980, pp. 89-107.

13. Henderson-Sellers, B., "Role of Eddy Diffusivity in Thermocline Formation," J. Env. Engineering Div., ASCE, Vol. 102, No. EE3, June, 1976, pp. 517-531.

14. Hicks, B.B., "On the Limiting Surface Temperature of Exposed Water Bodies," J. Geophysical Research, Vol. 80, Dec., 1975, pp. 5077-5081.

15. Hidy, G.M., and Plate, E.J., "Wind Action on Water Standing in a Laboratory Channel," J. Fluid Mech., Vol. 26, part 4, 1966, pp. 651-687.

16. Huber, W.C., Harleman, D.R.F., and Ryan, P.J., "Temperature Prediction in Stratified Reservoirs," J. Hydraulics Div., ASCE, Vol. 98, No. HY4, April, 1972, pp. 645-667.

17. Imberger, J. "Natural Convection in Shallow Cavity with Differentially Heated End Walls, Part 3, Experimental Results," J. Fluid Mech., Vol. 65, 1974, pp. 247-260.

18. Imberger, J., Patterson, J., Hebbert, B., Loh, I., "Dynamics of Reservoir of Medium Size," J. Hydraulics Div., Vol., 104, No. HY5, May, 1978, pp. 725-743.

19. Kato, H. and Phillips, O.M., "On the Penetration of a Turbulent Layer into Stratified Fluid," J. Fluid Mech., Vol. 37, part 4, 1969, pp. 643-655.

20. Keulegan, G.H., "An Experimental Study of the Motion of Saline Water from Locks into Fresh Water Channels," Nat. Bur. Standards Report 5168, 1957.

21. Koh, R.C.Y., "Viscous Stratified Flow Towards a Sink," J. Fluid Mech., Vol. 24, 1966, pp. 555-575.

22. Kreith, F., Principles of Heat Transfer, Intext Press, 1973.

23. Lee, K.K. and Liggett, J.A., "Computation for Circulation in Stratified Lakes," J. Hydraulics Div., ASCE, Vol. 96, No. HY10, Oct., 1970, pp. 2089-2115.

24. Liggett, J.A. and Hadjitheodorou, C., "Circulation in Shallow Homogeneous Lakes," J. Hydraulics Div., ASCE, Vol. 95, No. HY2, March, 1969, pp. 609-621.

25. Octavio, K.A.H., Jirka, G.H., and Harleman, D.R.F., "Vertical Heat Transport Mechanisms in Lakes and Reservoirs," Report No. 227, R.M. Parsons Laboratory, M.I.T., Aug., 1977.

26. Orlob, G.T. and Selna, L.G., "Temperature Variations in Deep Reservoirs," J. Hydraulics Div., ASCE, Vol. 96, No. HY2, Feb., 1970, pp. 291-409.

27. Paily, P.P., Macagno, E.O., and Kennedy, J.F., "Winter Regime Surface Heat Loss from Heated Streams," Iowa Institute of Hydraulic Research Report 155, Iowa City, March, 1974.

28. Phillips, O.M., "On Turbulent Convection Currents and the Circulation of the Red Sea," Deep Sea Research, Vol, 13, 1966, pp. 1149-1160.

29. Ryan, P.J. and Harleman, D.R.F., "Prediction of the Annual Cycle of Temperature Changes in a Stratified Lake or Reservoir; Mathematical Model and User's Manual," Report no. 137, R.M. Parsons Laboratory, M.I.T., 1971.

30. Ryan, P.J. and Harleman, D.R.F., "An Analytical and Experimental Study of Transient Cooling Pond Behavior," Report No. 161, R.M. Parsons Laboratory, M.I.T., 1973.

31. Scherer, C.R., "On the Efficient Allocation of Environmental Assimilative Capacity: The Case of Thermal Emissions to a Large Body of Water," Water Resources Research, Vol. 11, No. 1, Feb., 1975, pp. 180-181.

32. Spigel, R.H., "Wind Mixing in Lakes," Ph.D. Thesis, Univ. of Calif., Berkeley, 1978.

33. Stefan, H. and Ford, D.E., "Temperature Dynamics in Dimictic Lakes," J. Hydraulics Div., ASCE, Vol. 101, No. HY1, Jan., 1975, pp. 97-115.

34. Sturm, T.W., "An Analytical and Experimental Investigation of Density Currents in Sidearms of Cooling Ponds," Ph.D. Thesis, Univ. of Iowa, May, 1976.

35. Turner, J.S. and Kraus, E.B., "A One-Dimensional Model of the Seasonal Thermocline, I. A Laboratory Experiment and Its Interpretation," Tellus, Vol. 14, 1967, pp. 88-97.

36. Turner, J.A., Buoyancy Effects in Fluids, Cambridge Univ. Press, 1973.

37. Wu, Jin, "Wind-Induced Turbulent Entrainment Across a Stable Density Interface," J. Fluid Mech., Vol. 61, Part 2, pp. 275-287.

Appendix – Definition of Profile Constants

$$C_1 = \left(\int_0^1 f_T(\eta)\, f_u(\eta)\, d\eta \right)^{-1}$$

$$C_2 = 3 \int_0^1 \int_0^\eta [f_1(\eta) - f_1(1)]\, d\eta d\eta$$

$$C_3 = C_1 f_u(1)$$

$$C_4 = C_1 \int_{h/D}^1 f_u(\eta)\, d\eta$$

$$\text{where } f_1(\eta) = \int_0^\eta \int_1^\eta f_T(\eta)\, d\eta d\eta$$

$$f_u(\eta) = -\int_0^\eta \int_1^\eta \int_1^\eta f_T(\eta)\, d\eta d\eta d\eta - \frac{C_2}{2}\, \eta^2 + C_2 \eta$$

Appendix: Table 3.-Measured Temperatures in
St. Joseph's Lake

(a) 1976 Data; Temperatures in $^{\circ}$C.

Station	Depth* ft	6/29	7/27	8/3	8/10	8/17	8/31	9/21	10/19
					Dates				
A1	10		27.0	25.	23.5	23.0	23.5	22.0	
	5		28.0	25.	23.5	24.0	23.5	22.0	
	0		28.5	25.5	24.0	24.0	23.5	22.0	
B	38	11.0	14.0	12.0	13.0	13.5	14.0	14.0	16.0
	35	12.0	14.0	12.0	13.0	14.5	14.0	20.0	16.0
	30	15.5	21.0	22.5	22.0	22.0	22.5	20.5	16.0
	25	23.0	24.0	23.5	23.0	23.0	23.0	21.0	16.0
	20	23.5	26.0	24.5	23.0	23.5	23.0	21.5	16.0
	15	24.5	26.0	25.0	23.0	24.0	23.5	22.0	16.0
	10	25.0	27.0	25.0	23.5	24.0	23.5	22.0	16.0
	5	25.0	27.0	25.0	24.0	24.0	24.0	22.0	16.0
	0	25.5	28.0	25.0	24.0	24.0	24.0	22.0	16.0
C	39	9.0	10.0	12.5	11.0	12.0	10.0	13.0	16.0
	35	9.5	11.5	13.0	12.5	14.0	14.0	18.0	16.0
	30	15.0	20.0	22.0	22.0	22.0	22.0	20.5	16.0
	25	22.0	25.0	24.0	23.0	23.0	23.0	21.0	16.0
	20	23.5	26.0	24.5	23.0	23.5	23.0	21.5	16.0
	15	24.0	26.5	25.0	23.0	23.5	23.5	22.0	16.0
	10	24.5	27.0	25.0	23.5	24.0	23.5	22.0	16.0
	5	25.0	27.0	25.0	23.5	24.0	24.0	22.0	16.0
	0	25.5	28.5	25.5	24.0	24.0	24.0	22.0	16.0
D	30		24.5	24.0	23.0	23.5	23.0	21.0	16.0
	25		25.5	24.0	23.0	23.5	23.0	21.5	16.5
	20	24.0	26.5	24.5	23.0	23.5	23.0	22.0	16.5
	15	24.0	27.0	25.0	23.0	24.0	23.0	22.0	16.5
	10	24.5	27.0	25.0	24.0	24.0	23.5	22.0	16.5
	5	25.0	27.5	25.0	24.0	24.0	24.0	22.0	16.5
	0	26.5	29.0	26.0	25.0	25.0	24.0	22.0	16.5
H	4	25.5	29.0	25.5	24.0	25.0	24.0	22.0	17.0
	2	27.0	29.0	26.0	24.5	25.0	24.0	23.0	17.0
	0	28.0	31.0	27.0	27.0	26.0	26.0	23.0	17.5
I	4	26.0	29.0	26.0	24.5	25.0	24.0	23.0	
	2	26.0	29.0	26.5	25.0	26.0	25.0	24.0	
	0	28.0	33.0	28.0	28.0	27.0	27.5	24.5	17.5

\# Surface temperatures measured at a depth
of approximately 4 in.

(b) <u>1978 Data;</u> <u>Temperatures in °F.</u>

Station	Depth ft	4/25	5/4	5/10	6/3	6/9	7/17	8/8	9/6
A2	23			51.0	66.0	70.5	75.5	76.0	76.0
	20			52.0	74.0	72.0	75.5	76.0	76.5
	15			55.0	75.5	72.5	76.0	76.0	77.0
	10			56.0	76.0	74.0	76.5	77.0	77.0
	5			56.0	76.0	75.0	78.0	78.0	78.0
	1			56.0	77.0	77.0	80.0	79.0	78.0
C	39	44.5	44.0	45.0	47.0	47.0	49.0	51.0	52.0
	35	44.5	44.0	45.0	47.0	47.0	50.5	54.0	56.0
	30	44.5	44.0	45.0	47.0	48.0	64.5	70.0	72.0
	25	46.0	46.5	46.5	55.0	66.0	72.0	74.0	74.0
	20	49.5	50.0	53.0	71.0	69.5	73.5	74.0	74.5
	15	50.0	55.0	55.0	73.0	71.0	75.0	74.5	75.0
	10	50.0	55.0	55.0	74.0	72.5	75.5	75.5	75.5
	5	54.0	55.5	55.0	75.0	73.0	76.5	76.0	76.0
	1	54.0	55.5	56.0	76.0	76.0	78.0	78.0	76.5
D	29			45.0	50.0	51.0	71.5	73.0	74.5
	25			46.0	56.0	67.0	74.5	75.0	76.0
	20			53.0	72.0	71.0	75.0	75.5	76.5
	15			55.0	74.0	71.0	76.0	76.0	76.5
	10			55.0	74.5	72.0	76.5	76.5	77.0
	5			55.0	75.0	74.0	77.5	77.5	77.0
	1			56.0	77.0	76.0	79.0	79.0	78.5
E	24			52.0	54.0		75.0	75.5	76.0
	20			54.0	73.0	72.0	76.0	76.0	76.5
	15			55.0	74.0	72.5	76.5	76.0	77.0
	10			56.0	75.0	73.0	77.0	77.0	77.0
	5			56.0	75.0	75.0	77.5	77.5	77.5
	1			57.0	76.0	77.0	79.0	79.0	78.0
F	24			52.0		71.5	76.0	76.0	76.5
	20			54.0	73.5	72.0	76.0	76.0	76.5
	15			55.5	76.0	72.5	76.5	76.0	77.0
	10			56.0	76.0	73.0	77.0	77.0	77.0
	5			56.0	76.0	75.0	78.0	78.0	77.5
	1			57.0	77.0	77.0	80.0	79.0	78.5
G	3			58.0	77.0	76.5	79.0	78.5	78.0
	1			58.5	81.0	78.5	82.0	81.0	78.0
H	4	57.0		58.0	77.0	76.0	79.0	78.0	79.0
	2	58.0		58.0	78.0				
	1	59.0		59.0	81.0	78.5	82.0	80.0	79.0